The Journal of Membrane Biology (2019) 252:425–449
https://doi.org/10.1007/s00232-019-00095-0

# Quantum Mechanical and Molecular Mechanics Modeling of Membrane-Embedded Rhodopsins

**Mikhail N. Ryazantsev[1] · Dmitrii M. Nikolaev[2] · Andrey V. Struts[3,4] · Michael F. Brown[3,5]**

Received: 23 August 2019 / Accepted: 10 September 2019 / Published online: 30 September 2019


**Abstract**
Computational chemistry provides versatile methods for studying the properties and functioning of biological systems at different levels of precision and at different time scales. The aim of this article is to review the computational methodologies that are applicable to rhodopsins as archetypes for photoactive membrane proteins that are of great importance both in nature and in modern technologies. For each class of computational techniques, from methods that use quantum mechanics for simulating rhodopsin photophysics to less-accurate coarse-grained methodologies used for long-scale protein dynamics, we consider possible applications and the main directions for improvement.

**Keywords** GPCR · Membrane · Molecular dynamics · Protein dynamics · Quantum mechanics · Retinal

## Introduction

Rhodopsins constitute a large class of membrane proteins that are found in many species, from ancient protobacteria (archea) to human beings. As the cofactor, they use the retinal chromophore or its derivatives, which are covalently bound to a seven-transmembrane helix protein, opsin. Retinylidene proteins function as light sensors, ion pumps, and even thermo- and chemosensors (Govorunova et al. 2017; Rotov et al. 2018; Smith 2010). After photon absorption or other types of cofactor activation, isomerization of the chromophore triggers a series of subsequent structural reorganizations of the protein. Both physical properties, such as electronic absorption wavelength, and the functions of the different rhodopsins are determined by the primary structure of the protein. Rhodopsin primary structure modification allows for functional diversification of these proteins, which are widely utilized both in nature and technology (Govorunova et al. 2016; Hochbaum et al. 2014; Nikolaev et al. 2019b).

For this reason, understanding the correlation between structure and function in opsins and rhodopsins is an important task in the biophysical research field. To accomplish such a goal, both experimental and computational approaches are applied. Experimental techniques can reveal many important details of rhodopsin structure, starting from the primary sequence up to oligomeric aggregates within a membrane environment; they can detect and characterize intermediates of the rhodopsin photosequence; and determine the timescale for their rising and disappearing starting from femtoseconds up to hours. These techniques include X-ray crystallography (Gushchin et al. 2015; Volkov et al. 2017); nuclear magnetic resonance (NMR) (Jensen et al. 2014; Mertz et al. 2012), Raman (Gellini et al. 2000; Saint Clair et al. 2012b), electronic (UV–visible) (Maclaurin et al. 2013), circular dichroism (CD) (Thomas et al. 2009), and Fourier transform infrared (FTIR) spectroscopies (Chen et al. 2018; Hein et al. 2003; Saint Clair et al. 2012a), together with electron microscopy (Krebs et al. 2003) and neutron scattering (Perera et al. 2018; Shrestha et al. 2016). From another side, computational modeling offers an additional dimension for the understanding of rhodopsin structure and function. Computational models can both support

✉ Michael F. Brown
mfbrown@u.arizona.edu

1 Institute of Chemistry, Saint Petersburg State University, 26 Universitetskii pr, Saint Petersburg, Russia 198504

2 Saint-Petersburg Academic University – Nanotechnology Research and Education Centre RAS, Saint Petersburg, Russia 194021

3 Department of Chemistry and Biochemistry, University of Arizona, Tucson, AZ 85721, USA

4 Laboratory of Biomolecular NMR, Saint Petersburg State University, Saint Petersburg, Russia 199034

5 Department of Physics, University of Arizona, Tucson, AZ 85721, USA

the interpretations of experimental findings and provide additional insights with atomistic resolution. In this review, we provide the detailed description of the computational techniques that are used for rhodopsin modeling, starting from an evaluation of the local conformational dynamics based on the available X-ray structure and the primary sequence, up to the global protein dynamics on the millisecond time scale with coarse-grained approaches.

## Main Approaches and Methodologies Used for Computational Modeling of Opsins and Rhodopsins

More broadly, rhodopsins refer to the group of either homologous or nonhomologous proteins comprising an opsin apoprotein and a retinylidene chromophore. Contrary to their name, microbial rhodopsins occur not only in archaea and bacteria, but also in eukaryotes (such as algae). (Recall that prokaryotes are divided into two domains, archaea and bacteria, while eukaryotes comprise a third distinct life domain.) Prokaryotic rhodopsins include bacteriorhodopsins, archaerhodopsins, proteorhodopsins, xanthorhodopsins, halorhodopsins, and sensory rhodopsins; and unicellular algae and other eukaryotes contain channelrhodopsins. Various ion-translocating microbial rhodopsins find important applications in optogenetics, which uses light to modulate neuronal activity in cells genetically modified to express light-sensitive ion channels. Microbial rhodopsins are different from and are nonhomologous to any of the G-protein-coupled receptor (GPCR) families. The microbial rhodopsins have significant sequence homology to one another, yet they have no detectable homology to the GPCR family to which animal visual rhodopsins belong. Nevertheless, microbial rhodopsins and GPCRs are possibly evolutionarily related because of their analogous three-dimensional structures; they are members of the same superfamily.

Rhodopsin (visual purple) is the opsin with bound 11-*cis* retinal that is responsible for scotopic (dim light) vision in vertebrate animals. The cofactor retinal is bound as a Schiff base to a conserved lysine residue on the seventh transmembrane helix (H7). Vertebrate visual opsins include not only rhodopsin, but also the cone opsins, which are the color-sensing pigments. Depending on the number of cone opsins (colors detected) animals are classified as dichromats (dogs, cats), trichromats (humans), and tetrachromats (some birds and mantis shrimps). In addition, melanopsin is found in the retina and is involved in circadian rhythms, and pinopsin occurs in the pineal gland of the brain, which produces melatonin, a serotonin-derived hormone that modulates sleep patterns in both circadian and seasonal light cycles. Visual rhodopsin and the vertebrate opsins in animals are members of the large GPCR gene family. The *Rhodopsin* class (Family A) GPCRs includes the opioid receptors, the cannabinoid receptors, dopamine receptors, and the $\beta$-adrenergic receptors (Weis and Kobilka 2018).

### Initial Construction of Three-Dimensional Models for Rhodopsin Proteins

In order to perform computational analysis of the properties and dynamics for any protein system, including opsins and rhodopsins, a high-quality three-dimensional structure of the protein is required (Fig. 1 shows an example of dark- and light-activated rhodopsins). In most studies, an X-ray structure of the target visual rhodopsin pigment or microbial rhodopsin is used. However, experimental structures are not always available for rhodopsins, or their intermediates and mutants. In this case, a three-dimensional structure has to be predicted starting from the corresponding protein amino-acid sequence, with methodologies described in the next section. To complete the three-dimensional model, either constructed based on the X-ray structure, or predicted starting from the amino-acid sequence, one has to determine the protonation states of all the titratable residues. In addition, one must predict the locations of the water molecules that can be only partially resolved by X-ray crystallography.

### Prediction of Three-Dimensional Rhodopsin Structure

If an X-ray structure is available, the optimal strategy is to begin with this conformation and proceed to the next steps

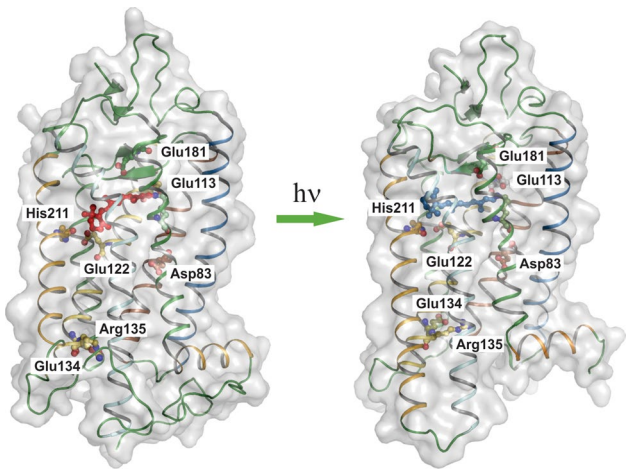


**Fig. 1** X-ray structures of rhodopsin in the dark (left, PDB code 1U19) and active metarhodopsin-II states (right, PDB code 3PQR). Retinal ligand is shown in red for the dark state and in blue for the active metarhodopsin-II state. Major amino-acid residues involved in rearrangement of hydrogen-bonding networks leading to activation are indicated

that are described in the "Prediction of Water Molecule Localizations"; "Prediction of the Protonation State for Titratable Residues"; and "Insertion into a Lipid Membrane Environment" sections. Otherwise, one has to predict a three-dimensional structure of the protein based on its primary amino-acid sequence. For protein structure prediction, two general strategies are applied—either ab initio or homology modeling (Dorn et al. 2014). In the ab initio approach, the protein folding process is modeled under the guidance of a physically realistic energy function by sampling the protein conformational space using molecular dynamics or Monte Carlo simulations. Even though this approach is more fundamental, it requires the investigation of a huge conformational space, and, therefore, it is very computationally expensive (Dorn et al. 2014; Khan et al. 2016; Lee et al. 2017). Accordingly, the ab initio approach is rarely used alone, giving preference to homology modeling methods that can include ab initio modeling as an integral part (Wu et al. 2007).

Homology modeling methods use the X-ray structures of close homologs as an initial approximation (template). To choose the appropriate template, alignment of the primary sequences of the target protein and the possible template protein is carried out, and the template protein with the most similar amino-acid sequence is selected (Chothia and Lesk 1986). Usually, to find the appropriate template protein(s) and perform accurate sequence alignment, automatic algorithms that search the databases of protein structures are used (Hill and Deane 2012; Söding 2004; Wu and Zhang 2008). To predict the target structure on the basis of the selected template, the following approaches are generally applied.

(*i*) In the global approach to structure building, at the first step, a complete backbone structure is modeled, and then it is reorganized under the constraint of a specific energy function. To build the initial conformation, the following algorithm is usually applied. The structures of the conserved regions are extracted from the template(s) and reorganized in the proper order. The conserved regions are defined on the basis of the target-template sequence alignment. The conformation of nonconserved regions is generated using the ab initio approach (Eswar et al. 2006; Roy et al. 2010; Song et al. 2013). Next, the conformational search is performed using Monte Carlo or molecular dynamics-based approaches with the guidance of a specific energy function. Usually, three kinds of energy functions are used and combined: physically based energy functions (Alford et al. 2017), statistically driven energy functions (Yang et al. 2015) and energy functions that represent template-derived spatial constraints (Eswar et al. 2006). The sampling procedure can be aimed at the optimization of either the energy or free energy of the system. In the latter case, the conformations generated during the sampling procedure are clustered (on the basis of geometrical similarity) (Zhang and Skolnick 2004). As a general rule, it is assumed that the largest clusters correspond to the conformations with the lowest free energy. Then, the centroids of the largest clusters are generated as prefinal models. To obtain the final conformations, the prefinal models are additionally optimized to avoid steric clashes that may occur during the generation of the centroid models (Yang et al. 2015; Yang and Zhang 2015).

(*ii*) For local structure building, the core of the structure is extracted from the template (for membrane proteins, it is the center of the transmembrane region) (Ebejer et al. 2013; Kelm et al. 2010). Afterward, the structure is completed on a residue-by-residue basis. Following the addition of each amino acid, local optimization of its orientation is performed to predict its most optimal position. Usually, during the initial conformational search, only the backbone atoms are modeled, and the side chains are represented only by their centers of mass (Yang et al. 2015). When the final conformation is predicted, the side chains are added from specific rotamer libraries. The orientations of the side chains that do not lead to the emergence of steric clashes are selected, and the final energy optimization is performed (Xu and Zhang 2011).

In a recent study (Nikolaev et al. 2018), the performance of several modern homology modeling approaches that combine algorithms for structural construction and optimization have been compared. A set of 24 rhodopsins, both visual and archaeal, were investigated (Nikolaev et al. 2018). This study demonstrated that the correct choice and usage of modern homology methodologies allows for accurate prediction of average structural properties of rhodopsin proteins (Yang and Zhang 2015). Even then, to evaluate the quality of homology modeling-based rhodopsins for subsequent computational modeling, further investigations are needed. It is also worth mentioning that all modern homology modeling algorithms do not consider the retinal moiety, and, for this reason, the orientation of side chains in the retinal-binding cavity can be incorrect. Although these inaccuracies can lead to steric clashes when the retinal cofactor is inserted in the model, optimization of retinal geometry on the molecular mechanics (MM) level can be applied to overcome these problems (Nikolaev et al. 2018).

## Prediction of Water Molecule Localizations

When experimental data about the locations of water molecules in rhodopsins are not available or incomplete, computational algorithms for predicting water molecules in protein cavities are applied. The pipeline of such algorithms can be divided into two general steps: finding the possible water

positions; and evaluation of the propensity of positioning the water molecules at the defined locations.

(*i*) Initially, comparatively simple approaches that involved finding protein cavities with a probe radius and energy minimization of water molecules in the cavity were applied (Zhang and Hermans 1996). With the development of docking algorithms, stochastic approaches were introduced (Trott and Olson 2010). These approaches combine global and local optimization techniques to find all possible water positions in a given cavity with subsequent clustering of the possible positions (Trott and Olson 2010).

(*ii*) To evaluate the propensity of a water molecule to be placed at a certain location inside a protein cavity, two approaches are used. In the first approach, implemented in the Dowser (Zhang and Hermans 1996) and Dowser++ (Morozenko and Stuchebrukhov 2016) algorithms, the potential energy of interaction between the water molecule and the environment is calculated. The proposed energy function includes terms that consider van der Waals interactions (approximated by the 6–12 Lennard-Jones potential), electrostatic interactions with charges on protein atoms, and electrostatic interactions with water molecules inside the same cavity. In all the water prediction algorithms, Marsili–Gasteiger partial charges are usually applied for the calculation of electrostatic interactions (Gasteiger and Marsili 1980). This approach does not take into account the entropy of the water molecules inside the cavity. However, the developers of these algorithms assume that the entropy factor is small (~ 1 kcal/mol) (Morozenko et al. 2014). If the value of the potential energy describing the interaction of the water molecule with the cavity environment is less than a certain threshold, e.g., − 10 kcal/mol in Dowser and − 4 kcal/mol in Dowser++, the water molecule is accepted.

In the second approach, implemented in the WaterDock (Ross et al. 2012) and WaterDock 2.0 (Sridhar et al. 2017) programs, an empirical energy function that describes the free energy of placing a water molecule inside the target cavity, i.e., including the entropy factor, is proposed. This energy function involves terms that take into account steric, hydrophobic, and hydrogen-bonding interactions, and is essentially empirical—it is not based on the actual physical potentials (Ross et al. 2012; Trott and Olson 2010). Thus, to predict water positions in protein cavities, modern algorithms analyze each possible cavity by testing all possible positions of water molecules inside it. The possible water positions are scored and clustered, generating a small number of final variants. Finally, the energy or free energy of the possible water molecules inside a cavity is calculated, and those water molecules that are energetically unfavorable are removed. It should be mentioned that for rhodopsins, comparative studies of these methodologies have not yet been conducted, and further investigations are needed to fill this gap. To further improve the quality of water prediction, more accurate estimation of the water–protein interaction energy should be considered. Such approaches can estimate the free energy of transferring a water molecule from the bulk to a specific site in the protein cavity, and optimize the position of a water molecule in the cavity by free energy minimization. While free energy calculations are still computationally expensive, and cannot be applied to test all protein cavities, they can be used in critical cases, i.e., when highly structured functionally important water clusters are concerned. Besides, to develop strategies for improvement, extensive benchmarks that compare existing algorithms should be performed. To our knowledge, the algorithms for water prediction have never been tested on a large class of proteins. Rather, the test pools were limited by the small amount of globular proteins with sufficient numbers of water molecules resolved in the X-ray structure.

## Prediction of the Protonation State for Titratable Residues

To predict the protonation state of titratable residues, in proteins p$K_A$ calculations of these residues are performed. The most widely applied algorithms for p$K_A$ calculations imply empirical implicit approaches. For example, the algorithm implemented in the PROPKA program (Olsson et al. 2011) takes into account electrostatic interactions of the ionizable residues with charges and dipoles of the protein environment, as well as van der Waals interactions. In addition, the algorithm considers the hydrogen bonding and desolvation energy, i.e., the free energy of transferring the amino acid from the bulk to the protein environment. While MM-based or QM/MM-based calculations of such energy terms are computationally expensive, the algorithm implemented in PROPKA applies empirical parameters (Olsson et al. 2011; Rostkowski et al. 2011). Recently, a new method for predicting the protonation states was developed and implemented in the Rosetta program package (Kaufmann et al. 2010). It defines the most energetically favorable states during sampling under the guidance of the modified force field. The modification required adding a term that considers the probability of protonation at a given pH to the potential energy function (Kilambi and Gray 2012). In other strategies, calculations of all-atom MD trajectories for the protein in explicit or implicit solvents, as well as QM/MM calculations, have been applied to evaluate p$K_A$ values. In addition, modern algorithms apply Monte Carlo sampling to optimize the hydrogen-bonding network in the protein (Dolinsky et al. 2004, 2007). These approaches are computationally

expensive (Schaefer et al. 2005; Simonson et al. 2004), but they can be indispensible in some challenging cases, and their usage will be increasing. Prediction of the protonation state of titratable residues is a general biological problem of special importance, and these methodologies are always improving.

The major problem of all p$K_A$ calculation approaches is that they evaluate p$K_A$ values only for an immobile or "frozen" protein conformation. However, during the dynamics occurring under the natural conditions, the p$K_A$ values change with the alteration of protein conformation, meaning that the protonation state of the ionizable residue also fluctuates. For this reason, it would be much more natural to apply algorithms for p$K_A$ calculation and protonation of titratable residues "on the fly" during the molecular dynamics simulations. Such an approach is partially implemented in constant-pH molecular dynamics (Khandogin and Brooks 2005). Even then, modern constant-pH MD algorithms do not apply accurate methods of the p$K_A$ estimation. Thus, the combination of the most accurate p$K_A$ calculations with constant-pH molecular dynamics simulations is a possible direction of improvement in this field.

### Insertion into a Lipid Membrane Environment

In order to take the natural environment of membrane proteins into account, a model constructed as described above has to be inserted into the lipid bilayer. Two approaches are commonly used for this purpose. In the first approach, the membrane bilayer is implicitly considered by applying a membrane-imitating electrostatic field (Im et al. 2003; Mori et al. 2016; Ulmschneider and Ulmschneider 2009). Even though this approach seems to be less accurate than the explicit membrane modeling, it has two important advantages. First, an implicit membrane model greatly reduces the computational cost of the calculations, and allows for more extensive sampling (Grossfield 2008). Second, the implicit membrane imitates the average electrostatics, which is closer to the natural conditions, thus enabling better investigation of the rhodopsin conformational space in the lipid membrane environment (Feig 2008; Ulmschneider and Ulmschneider 2009).

On the other hand, explicit parameters for different types of lipid bilayers have been extensively developed in the last decade (Cordomí et al. 2012; Jämbeck and Lyubartsev 2012; Klauda et al. 2010; Pastor and MacKerell 2011). These include saturated (e.g., DMPC, DPPC), and unsaturated (e.g., DOPC, POPC) lipid types (Jämbeck and Lyubartsev 2012). Among the most recent advances in this area, the Lipids14 membrane parameters should be mentioned (Dickson et al. 2014). In this work, the authors developed the optimal lipid parameters that allow for accurate reproduction of natural thermodynamic and dynamic properties of lipid bilayers during short and long MD simulations. These parameters are compatible with the AMBER force field (Lindorff-Larsen et al. 2010). For the CHARMM force field, appropriate lipid parameters are also available (Leonard et al. 2018; Pastor and MacKerell 2011).

Another problem related with the explicit membrane modeling is the development of accurate algorithms for insertion of the protein into a membrane lipid bilayer. The most straightforward approach, which is commonly applied, is cutting out a cavity of the proper size in the preequilibrated lipid bilayer, inserting a membrane protein inside the cavity, and performing accurate optimization of the whole system. Recently, a new approach, implemented in LAMBADA and InflateGro algorithms, was proposed (Schmidt and Kandt 2012). Here, the relative orientation of the membrane protein and the lipid bilayer is determined on the basis of the protein hydrophobicity profile. Lipid molecules "inflate" in order to provide enough space among themselves for the protein. Afterward, the lipid bilayer shrinks back to envelop the protein without inducing any steric clashes. The authors showed that implementation of this algorithm allows for physically realistic membrane embedding, even if a heterogeneous membrane is considered. For rhodopsins, all these algorithms can be applied on a regular basis at present.

## Computational Strategies that can be Applied for Rhodopsin Modeling

Here we consider visible rhodopsins and microbial rhodopsins for the purposes of illustration. As mentioned above, visual rhodopsin is the archetype for the large *Rhodopsin* class of (Family A) G-protein-coupled receptors, with an increasing number of X-ray and cryo-electron microscopy structures becoming available. Because this largest class of vertebrate membrane proteins has around 800 members, modeling approaches may be necessary for those members whose tertiary structures are not currently available.

### Hierarchy of Computational Models

To model the physical, chemical, and biological properties of rhodopsin proteins, all the main approaches of computational chemistry and biophysics can be applied. The difficulties that have to be overcome for successful implementation of these computational methodologies are typical for flexible molecular systems of this size (Fig. 2).

(*i*) First, due to the relatively large size of rhodopsin proteins, the most general approaches, i.e., employing ab initio quantum chemistry or density functional theory (DFT), can be used only as a part of a hybrid quantum mechanics/

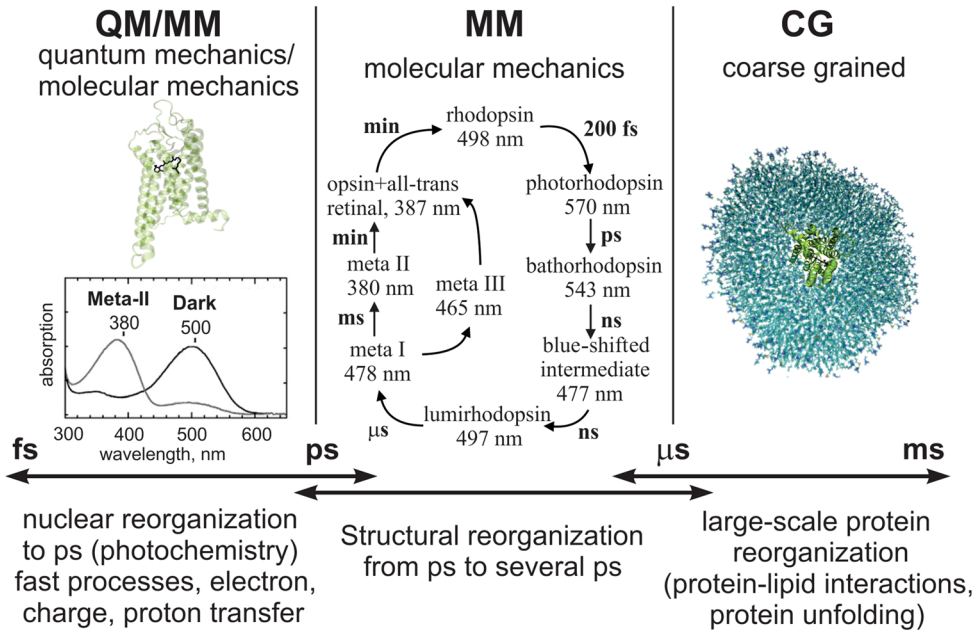


**Fig. 2** Hierarchy of rhodopsin computational models. (left) Hybrid quantum mechanics/molecular mechanics (QM/MM) models are used to model intrinsically quantum mechanical processes, such as light absorption, or electron, proton, or energy transfer. (center) Molecular mechanics models are used to simulate medium- and long time-scale protein dynamics (up to hundreds of $\mu$s) or to perform extensive conformational searches. (right) Coarse-grained simulations are used to simulate even longer time-scale processes in proteins and protein–lipid complexes (up to several ms)

molecular mechanics (QM/MM) model. In such QM/MM models, a part of the protein, usually the chromophore, is described at the quantum mechanics level; and the rest of the protein is treated with a molecular mechanics force field. Two main approaches, subtractive and additive, are used to couple the QM and MM parts together (for details, see refs (Chung et al. 2015; Lin and Truhlar 2007; Senn and Thiel 2009) and the section below). Another option is to implement a pure molecular mechanics (MM) model or even a coarse-grained (CG) model. However, a QM/MM model cannot be displaced by a pure MM model if one wants to model "intrinsically" quantum mechanical processes, such as light absorption, electron, proton, or energy transfer, due to the difficulties in obtaining high-quality MM parameters for modeling of chemical reactions.

(*ii*) Second, again due to the comparatively large sizes of these proteins and their relatively high flexibility, one has to take the entropy factor into account even for modeling stationary properties. It requires extensive conformational searches with molecular dynamics or stochastic approaches, i.e., calculations of energies for substantial numbers of conformations and, if molecular dynamics are the method of choice, also the forces. The molecular dynamics approach also has to be used if one wants to model the evolution of the system over time. Obviously, more expensive QM/MM approaches can be applied only to model relatively short trajectories, starting from fs to ps. Still, the MM or CG models allow one to model the evolution of a system up to ms, and they are also indispensable for extensive conformational searches and, therefore, the evaluation of the Gibbs free energy.

## Classical Force Fields: Types and Parameterization

The calculation of energies and forces (gradients) is one of the central problems for quantum chemistry, and a number of both ab initio and DFT methodologies are available to perform this task. But even semiempirical ab intio and DFT methods are relatively expensive, and allow only calculations of relatively short trajectories. For modeling long-time events, or for extensive conformational space exploring, it is still much more practical to use the approximation of the potential energy surface of the molecular system in its low energy region, i.e., the so-called molecular mechanics (MM) approach. Setting the potential energy function for the MD calculations requires determination of its functional form. The most common approach is to use a potential energy function $U$ that will approximate the actual physical interactions between atoms (Lindorff-Larsen et al. 2010). Usually the potential includes van der Waals (approximated by a 6–12 Lennard-Jones potential) and Coulombic nonbonded interactions between atoms, and the bonded interactions between couples, triples, and tetrads of atoms. Many variations of these functional forms have been proposed, and they, together with experimentally derived parameters, define a force field. For example, the functional form of the general AMBER force field (Cornell et al. 1995; Wang et al. 2004) written in terms of potential energy reads:

$$U(\mathbf{r}) = \sum_{\text{bonds}} \frac{k_{ij}^{b}}{2}(l_{ij} - l_{ij}^{0})^2 + \sum_{\text{angles}} \frac{k_{ijm}^{a}}{2}(\theta_{ijm} - \theta_{ijm}^{0})^2 + \sum_{\text{torsions}} \frac{k_{ijmp}^{t}}{2}\left(1 + \cos(n\varphi_{ijmp} - \delta)\right) + \sum_{LJ} 4\varepsilon_{ij}\left(\frac{R_{ij}^{12}}{r_{ij}^{12}} - \frac{R_{ij}^{6}}{r_{ij}^{6}}\right) + \sum_{\text{Coulomb}} \frac{q_i q_j}{r_{ij}} \quad (1)$$

where **r** represents the Cartesian coordinates of the molecular system. The first term describes the bond stretches, $l_{ij}^{0}$ is the equilibrium distance between covalently bound atoms $i$ and $j$, and $k_{ij}^{b}$ is the bond force constant. The second term describes the bending of angles between three bonded atoms, $i$, $j$, and $m$, where $\theta_{ijm}^{0}$ is the equilibrium value for the corresponding angle, and $k_{ijm}^{a}$ is the bending force constant. The third term describes the torsional rotation of four bonded atoms around the corresponding central bond. Here, $\varphi_{ijmp}$ is the dihedral angle, $n$ is the multiplicity of the function, and $\delta$ is the phase shift. The final two terms describe the nonbonded van der Waals and Coulombic interactions.

Another widely used force field, OPLS, has the same functional form as the AMBER force field, with the only difference in the term for torsional rotation, which is described as a Fourier series of cosine functions (Kaminski et al. 2001). The variations can also include introduction of a cosine-based harmonic potential for the angles between bonded atoms, as in the case of the GROMOS force field (Oostenbrink et al. 2004). In other potentials, additional terms are often added to obtain a better approximation of the potential energy surface of the molecular system. Thus, in the CHARMM force field (Vanommeslaeghe et al. 2010), a harmonic term $k(\gamma - \gamma_0)^2$ that treats out-of-plane bending motion is introduced to keep certain groups planar. Furthermore, an additional harmonic Urey–Bradley potential is included that depends on the distance between the 1–3 bonded atoms to approximate the angle bending more accurately. Recent versions of the CHARMM force field also include grid-based energy correction mapping for backbone dihedral angles (CMAP) (Mackerell et al. 2004). As described above, defining the values for all the constants (parameters) is performed during the parametrization procedure. While the parameters for standard amino acids are constantly updated and already have good accuracy (Klauda et al. 2010; Lindorff-Larsen et al. 2010), the parametrization of nonstandard cofactors, e.g., retinal, is not very accurate to date, and requires further development (Mertz et al. 2011; Zhu et al. 2013).

## Parameterization for the Retinal Cofactor

To correctly model the retinal chromophore including its structure and dynamics at the molecular mechanics (MM) level, an accurate force field parameter set is required. Usually, the development and optimization of force field parameters is performed by fitting the results of molecular mechanics calculations to the results of quantum chemical calculations. The accuracy of the parameters can be also evaluated by the ability of models based on these parameters to correctly reproduce experimental data (X-ray or NMR structures, Raman or CD spectroscopic results) (Ferrand et al. 1993; Hamanaka et al. 1972; Zhou et al. 1993).

One of the first parameter sets for retinal was based on ab initio (HF/6-31G* and MP2/6-31G*) calculations of butadiene geometry and rotational energy barriers, which were extrapolated to the larger retinal moiety. In further studies, Nina et al. (1995) considered the energy surfaces for hydrogen bonds between the retinylidene Schiff base moiety and the water molecules in the retinal binding pocket as experimentally observed in bacteriorhodopsin (De Groot et al. 1990; Harbison et al. 1988). In both cases, the parameter sets were developed for the CHARMM force field (Cornell et al. 1995). Baudry et al. calculated ab initio the conformational energies of several model compounds that represented the parts of retinal (Baudry et al. 1997, 1999). Specifically, the Gibbs free energy differences between different conformations (corresponding to all-*trans*, 13-*trans*-15-*cis*, 13-*cis*-15-*trans*, (13,15)-*cis* retinal) were calculated at the MM level using an umbrella sampling approach, and were compared to the results of ab initio RHF/6-31G* and MP2/6-31G* calculations. In other studies, the parameter sets were developed on the basis of DFT calculations (B3lyp/6-31G*) of proton transfer and isomerization processes for different Schiff base models, including the complete retinal Schiff base model, in different environments (Tajkhorshid et al. 1997; Tajkhorshid and Suhai 2000). The comparison of these two parameter sets (developed on the basis of RHF/6-31G* Gibbs free energy calculations and DFT calculations) showed that the latter parameter set demonstrated higher isomerization energy barriers (Tajkhorshid et al. 2000).

As a means of improving the existing parameter sets, Hayashi et al. performed a QM/MM study of the retinal dynamics (for the ground and excited states of the molecule) in a bacteriorhodopsin environment (Hayashi et al. 2002). On the basis of QM/MM results and the previous DFT-based parameter set (Tajkhorshid et al. 2000), they presented improved retinal parameters by introducing additional improper torsional functions and a new charge scheme calculated on the CASSCF level. Moreover, Hayashi et al. also introduced additional force field parameters that treated the interaction of the retinylidene Schiff base with the nearby water molecules. One should note that an earlier molecular dynamics study of squid rhodopsin showed

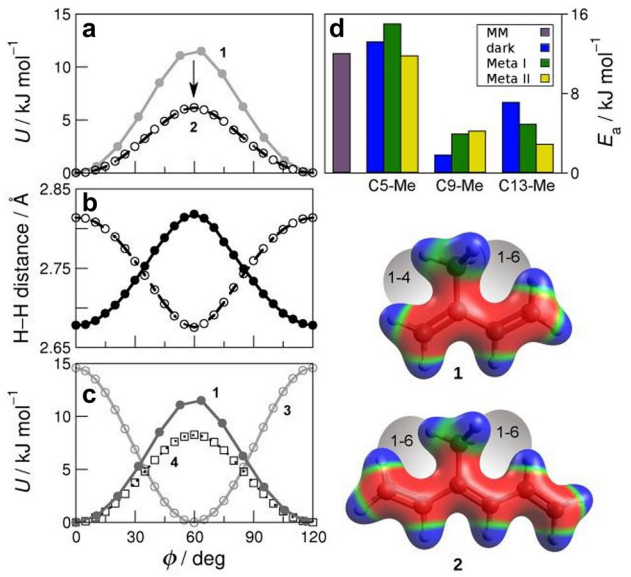


**Fig. 3** Torsional potential energy surfaces showing that 1–6 interactions affect retinal methyl rotation. **a** Comparison of QM (circles) and MM (lines) methyl torsion angle energies in compounds 1 and 2. **b** 1–6 distance in compound 2 between methyl hydrogen and C1 vinyl hydrogen (closed) and C5 vinyl hydrogen (open). **c** QM energy as a function of methyl torsion angle in compounds 1, 3 (propane), and 4 (propene). **d** Activation energies ($E_a$) for C5-, C9-, and C13-methyl groups from $^2$H NMR data for the dark, metarhodopsin-I, and metarhodopsin-II states of rhodopsin compared to a typical methyl dihedral energy barrier in a molecular mechanics force field. Steric interactions and electrostatic potentials are shown mapped to surfaces of 1 and 2. Adapted from Mertz et al. (2011) with permission from Elsevier

that the DFT-based parameter set (Tajkhorshid and Suhai 2000) slightly overestimates the planarity of the retinal Schiff base, making even the $\beta$-ionone ring coplanar with the polyene chain (Jardón-Valadez et al. 2010). In a recent study, the influence of different factors, including the applied QM methodology, selected moiety of the retinal Schiff base for the QM calculations of the final MM torsion parameters, and the resulting planarity of the chromophore was thoroughly investigated (Bondar et al. 2011). Further calculations of the retinal torsional energy landscape revealed the significance of the retinal methyl groups (Khandogin and Brooks 2005; Mertz et al. 2011; Struts et al. 2011). It follows that to reproduce the proper planar structure and isomerization dynamics of the retinal Schiff base, each methyl group should be treated individually (Struts et al. 2011). Intraretinal rotational potentials for the methyl groups change upon isomerization and deprotonation. More symmetric local structures correspond to lower rotational barriers (Fig. 3). These results have facilitated the development of an improved parameter set (Zhu et al. 2013). Here, the authors also introduced different torsional parameter sets for protonated and deprotonated retinal Schiff bases. Specifically, the MP2/6-31G* scans for each torsional degree of freedom were calculated for both protonated and deprotonated retinylidene Schiff bases.

Further development of the retinal parameter sets is related with automatic methodologies for force field parameterization on the basis of QM and QM/MM calculations. For example, in a recent study, the force matching approach was used to develop a new parameter set for retinal on the basis of QM/MM calculations for bovine visual rhodopsin (Doemer et al. 2013). Here, the algorithm minimizes the deviation of the forces acting on the retinal atoms between models obtained during the MM and QM/MM calculations. Recently, this approach was also implemented to study the photocycle of channelrhodopsin-2 (Ardevol and Hummer 2018). Thus, researchers were able to develop parameter sets for the retinal chromophore in the environment of interest. The extension of such automatic methodologies can be related with machine learning approaches that have been recently implemented to perform accurate parameterization of water molecules (Wang et al. 2012) and metal ions (Fracchia et al. 2017). The increase of accuracy is related with the improvement of the functional form of the force field that can include more complex effects, such as charge transfer and polarizability (Chen et al. 2008), and from the improvement of parameter sets. To develop such force fields, accurate sampling and accurate optimization procedures should be used. Specifically, the applied sampling procedure should generate structures that extensively represent the retinal conformational space in various environments (Fracchia et al. 2017).

## Molecular Dynamics Simulations

Molecular dynamics (MD) is the most general computational approach to study protein properties and evolution. Besides an exploration of the conformational space for Gibbs free energy calculations as described below, MD can be applied to study protein adaptation to specific environments, or to model the temporal evolution of the protein during the rhodopsin photosequence. During MD calculations, the nuclear motion is described by solving Newton's equations of motion. The forces acting on the atoms are calculated from the potential energy as follows:

$$F_i = -\frac{\mathrm{d}U}{\mathrm{d}\mathbf{r}_i}, \tag{2}$$

where $\mathbf{r}_i$ represents the Cartesian coordinates of the target atom, and $U$ is the potential energy function (potential energy surface, PES).

Most of the MD studies of rhodopsin dynamics have been aimed at investigating the structural changes that occur during the rhodopsin photocycle. For example, the coupling of the retinal motion with the global reorganization of the transmembrane helical bundle of rhodopsin, as well as the

extracellular and cytoplasmic loop regions, has been analyzed (Crozier et al. 2003; Kazmin et al. 2015; Kholmurodov et al. 2007). In several works, the computation of rhodopsin dynamics was combined with the results of NMR experiments to obtain more detailed information (Hornak et al. 2010; Lau et al. 2007; Leioatts et al. 2014; Mertz et al. 2012). Solid-state $^2$H NMR spectroscopy of deuterated lipid membranes recombined with rhodopsin together with MD simulations were used to study lipid–protein interactions and the effect of the membrane environment on rhodopsin activation and signal transduction (Huber et al. 2004). The solid-state NMR and MD simulation data indicated similar changes in order parameter profiles for the lipid acyl chains in recombinant membranes, as compared to membranes without rhodopsin. Here the important aspect is to confirm experimentally that the membrane structure is simulated correctly, before proceeding further with the analysis of all-atom simulations of rhodopsin-containing membranes. The authors concluded that the lipid membrane structure changes to match the hydrophobic lipid–protein interface, and thereby accommodate the transmembrane domain of the receptor. One of the MD simulations of the dark state of rhodopsin (Lau et al. 2007) has studied the retinal mobility, and has revealed that the $\beta$-ionone ring may rotate around the C6–C7 bond and may have multiple orientations in the dark state. Solid-state $^2$H NMR spectra of the C5-methyl group calculated based on the MD orientational distribution agree well with experimental solid-state $^2$H NMR spectra (Lau et al. 2007). Comparison of the $^2$H NMR spectra of the retinal methyl groups calculated from MD angular distribution with the experimental spectra was also used to evaluate proposed counterion models in the metarhodopsin-I state (Leioatts et al. 2014; Martínez-Mayorga et al. 2006; Mertz et al. 2012). The complex-counterion model showed good agreement with the experimental $^2$H NMR spectra, while the counterion-switch mechanism did not (Fig. 4). Furthermore, MD simulations have indicated that increased hydration of the receptor takes place already in the preactive metarhodopsin-I state (Grossfield 2008; Leioatts et al. 2014).

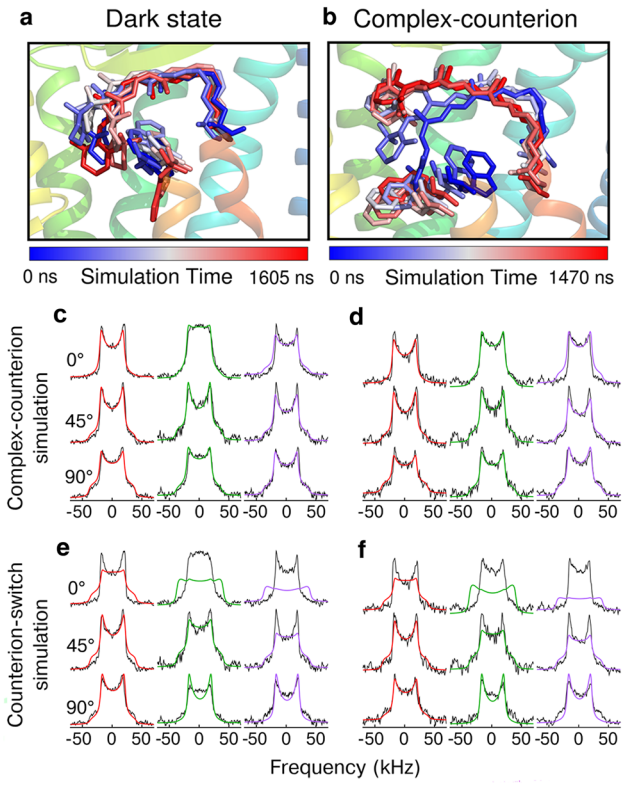


**Fig. 4** **a** Dark-state and **b** complex-counterion molecular dynamics MD simulations showing concerted transition and elongation of the retinal in rhodopsin's activation. Solid-state $^2$H NMR spectra calculated from MD simulations corroborate the complex-counterion model. Spectra were calculated from the complex-counterion (**c** and **d**), and counterion-switch (**e** and **f**) simulations. Simulation-based spectra are colored as follows: (red) C5-methyl, (green) C9-methyl, and (purple) C13-methyl group. These were compared to the dark-states (**c** and **e**) and metarhodopsin-I (**d** and **f**) experimental $^2$H solid-state NMR spectra (black). Adapted from Leioatts et al. (2014) with permission from ACS

## Retinal Isomerization

One of the approaches to trigger retinal isomerization during MD is the application of steered molecular dynamics (SMD) (Lemaître et al. 2005). In the SMD approach, an additional force is applied to quickly overcome the high energetic barrier of the isomerization. The authors (Lemaître et al. 2005) observed good correspondence for the inter-carbon distances (C10–C20, C11–C20, C8–C16, C8–C17, C8–C18) and dihedral angles of the retinal polyene chain obtained from $^{13}$C rotational-resonance NMR of metarhodopsin-I and calculated from a 10-ns MD simulation of rhodopsin after retinal isomerization. They concluded that the retinal relaxation after isomerization (lumirhodopsin or metarhodopsin-I states) extends by about 0.1–0.14 nm along its long molecular axis; however it maintains almost the same distance from helix H5 and helix H6. The NMR distance restraints obtained from $^{13}$C dipolar-assisted rotational-resonance (DARR) studies (Ahuja et al. 2009a, b; Patel et al. 2004) were used in guided MD simulations of the active metarhodopsin-II state. Throughout the course of the simulation, initial distances (corresponding to the crystal structure of rhodopsin in the dark state) were gradually changed toward experimental NMR distances characterizing active metarhodopsin-II. The MD simulation suggests that the retinal straightens in the metarhodopsin-II state, and the $\beta$-ionone ring translates by about 2 Å toward helix H5. The retinal motion leads to rearrangement of hydrogen bonding between His211 and Glu122 and around extracellular loop EL2, leading to its displacement toward the extracellular side. All these changes stabilize the active metarhodopsin-II

conformation. Notably, the $^{13}C$ DARR restraints (Ahuja et al. 2009a, b; Patel et al. 2004) do not support flipping of the retinal (rotation about its long axis by more than 90°) in the activation process. Meanwhile, two (Choe et al. 2011; Deupi et al. 2012) out of three (Choe et al. 2011; Deupi et al. 2012; Standfuss et al. 2011) crystallographic structures of active rhodopsin have indicated flipped retinal with the C9- and C13-methyl groups pointing toward the cytoplasmic side.

## Longer Time-Scale Molecular Dynamics Simulations

In a number of works, long time-scale MD simulations have been performed to investigate long-lasting processes in rhodopsin dynamics. Examples include studying rhodopsin deactivation processes, which involved modeling of retinal orientational changes during the metarhodopsin-II–metarhodopsin-I transition (Feng et al. 2015). The authors demonstrated the existence of a retinal flip about its long-axis that occurs in active rhodopsin under conditions favoring the inactive metarhodopsin-I state. In addition, $\mu$s sampling has been performed to study conformational ensembles of rhodopsin and opsin (Leioatts et al. 2014). It has been shown that upon photoisomerization, retinal destabilizes the inactive state of the receptor, whereas the active ensemble was more structurally homogenous. The active-like receptor without the ligand was on the contrary more structurally heterogeneous, and was able to transition from an active-like conformation to an inactive one. Nevertheless, the authors emphasized that the μs simulation is not long enough to explore transitions between the states in a statistically significant way.

### Lipid–Rhodopsin Interactions

Additional long time-scale MD simulations have been aimed at studying rhodopsin interactions with the surrounding lipids. For example, the processes of palmitoylation at specific cysteine sites have been thoroughly investigated (Olausson et al. 2012). In other research, the effect of the membrane environment on rhodopsin activation and signal transduction has been insightfully studied by Grossfield and coworkers (Grossfield 2011; Salas-Estrada et al. 2018). The question addressed by MD simulation studies of lipid–protein interactions is how the lipids modulate rhodopsin (or other GPCRs) function (Brown 1994, 2012, 2017). Is it through specific interactions or bulk properties of the lipid bilayer (Grossfield 2011)? Native membranes containing rhodopsin have a unique composition; they are enriched in polyunsaturated $\omega$-3 fatty acids and cholesterol. Polyunsaturated lipids stabilize the active rhodopsin state, while cholesterol shifts the equilibrium to the inactive metarhodpsin-I state. Early MD simulations (Feller et al. 2003) indicated a preference for the $\omega$-3 docosahexanoyl chains to interact with the protein. Later simulations identified distinct sites on the protein surface forming tight interactions with docosahexanoyl (DHA) (C22:6$\omega$-3) chains (Grossfield et al. 2006b), and suggested that the preference for polyunsaturated chains at the protein surface was entropically driven (Grossfield et al. 2006a). Recent MD simulations of rhodopsin in the dark, metarhodopsin-I, and metarhodopsin-II states, as well as in forms of inactive and active opsin in a SDPE lipid bilayer by Salas-Estrada et al. (2018), have revealed that both types of interactions (influence through macroscopic properties and specific binding-like events) are present in the rhodopsin-containing membranes. Correlations between the order parameters of saturated stearoyl (STEA) (C18:0) chains in the vicinity of rhodopsin and the state of the receptor were observed, indicating that more ordered and longer STEA chains correspond to an elongated active conformation of the protein (Salamon et al. 1999). On the other hand, comparatively long-lived (lasting > 500 ns) binding events for DHA and STEA chains were observed 1.7 times more often for DHA. Most of the long-lived DHA binding events occurred for the inactive rhodopsin conformation (Fig. 5). It was also shown that the proposed retinal flip may occur already in the dark state, and that it is correlated with lipid-protein interactions (Salas-Estrada et al. 2018).

### Microbial Rhodopsins

All-atom MD simulations have also been applied to investigate the proton transfer processes in channelrhodopsin (Takemoto et al. 2015). Here, the behavior of the protein pore during the 150-ns MD simulations was analyzed with models for the different protonation states of glutamate residues located in the vicinity of the protein active site. In another study, MD simulations were used to compare the stability of different retinal conformations in deep-red cone pigments of the American chameleon. The evaluation of the retinal energy during the MD simulations has revealed that these rhodopsins stabilize the 6-*s-trans* retinal conformation rather than standard 6-*s-cis* conformation of the $\beta$-ionone ring (Amora et al. 2008).

### G-Protein-Coupled Receptors

Besides visual and microbial rhodopsins, it is worth mentioning, that MD simulations are a powerful tool for investigation of activation/deactivation processes in various G-protein-coupled receptors, such as the $\beta_2$-adrenergic receptor (Dror et al. 2011; Latorraca et al. 2016; Nygaard et al. 2013), the $\mu$-opioid receptor (Huang et al. 2015), the serotonin receptor (Wacker et al. 2017), and others. For example, long MD trajectories starting from the active form of the receptor

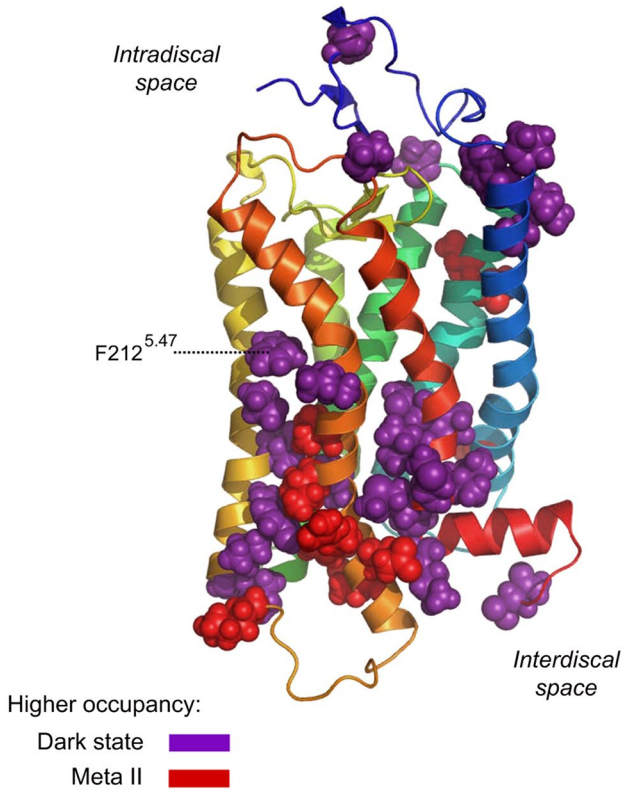


**Fig. 5** Protein residues with significantly different DHA occupancies in the dark and metarhodopsin-II states. Residues with higher occupancies in the dark state are colored purple, whereas residues with higher occupancies in the metarhodopsin-II state are colored red. Adapted from Salas-Estrada et al. (2018) with permission from Elsevier

have allowed simulating the conversion of the receptor into its inactive form (Dror et al. 2011; Nygaard et al. 2013). In other studies, long time-scale MD simulations were applied to extensively investigate the conformational space of the receptor, and thereby to define all possible stable conformations (Dror et al. 2009; Romo et al. 2010). In these studies, the receptor demonstrated two possible inactive conformations—a "locked" conformation with a salt bridge between the transmembrane alpha helices, and an open conformation without the salt bridge. Additional MD investigations showed that the transition between the "locked" and open conformations is regulated by the protonation state of a single aspartic acid that is located at a distance of 20 Å away from the salt bridge (Vanni et al. 2010). The interaction between the aspartic acid and the salt bridge entails the reorganization of several intermediate polar residues. An extensive investigation of the conformational space of the receptor was also performed by applying the accelerated MD approach (Tikhonova et al. 2013). A constant "boost" potential was applied to the dihedral angles that are included in the reaction coordinate of receptor activation. The "boost" potential enabled the transitions to occur between the active and inactive states, and allowed investigation of the influence of different antagonists on the conformational landscape of the receptor.

In addition, MD simulations have been applied to investigate the binding of different ligands to GPCRs, such as the $\beta_2$-adrenergic receptor. This method has allowed one to define the binding site and the main steps involved in the binding process (Kaszuba et al. 2010). In this way, it was shown that one of the key steps of the binding process is related with the reorganization and dislocation of water molecules at the binding site. Another study of the M2 muscarinic acetylcholine receptor by Dror et al. (2013) using atomic-level simulations has revealed binding sites for several allosteric modulators, and the mechanisms that contribute to positive and negative allosteric modulation of the classical ligand binding. It was shown that all modulators interact with clusters of aromatic residues within the extracellular vestibule of the receptor, located approximately 15 Å from the orthosteric ligand-binding site. Additional MD simulations of the adenosine $A_{2A}$ receptor, the $\beta_2$-adrenergic receptor, and visual rhodopsin have been used to study the functional role of internal water for receptor activation (Yuan et al. 2014). The simulations reveal that a continuous water channel forms only upon receptor activation (Leioatts et al. 2014).

A combination of molecular dynamics, radioligand binding, and thermostability experiments was used to investigate the role of a sodium ion binding site in the allosteric modulation of the human $A_{2A}$ adenosine receptor (Gutiérrez-de-Terán et al. 2013). It was revealed that sodium ions selectively bind and stabilize the inactive conformation of the receptor, and that the binding of sodium ions and agonists is mutually exclusive. Similar modulation was observed for the M3 muscarinic GPCR through long-timescale accelerated molecular dynamics (aMD) simulations (Miao et al. 2015). A subsequent MD study of the M2 muscarinic receptor (Vickery et al. 2018) has suggested a model for family-A GPCR activation, in which the conformational changes induced by the G-protein and agonist binding are accompanied by the intracellular transfer of an internally bound $Na^+$ ion. Explicit-solvent, all-atom molecular dynamics (MD) simulations of the adenosine $A_{2A}$ GPCR in a lipid bilayer were performed to study the effects of divalent cations on functional states of the receptor (Ye et al. 2018). The MD simulations suggested that high concentrations of cations bridge specific extracellular acidic residues, bringing transmembrane helices H5 and H6 together at the extracellular end, and driving open the G-protein-binding site. Molecular dynamics simulations have also been applied to study binding of the prototypical hallucinogen LSD to the human

5-$HT_{2B}$ receptor (Wacker et al. 2017). The MD simulations suggest that slow binding kinetics of LSD may be due to a "lid" formed by extracellular loop EL2 at the entrance to the binding pocket.

The question of how GPCRs catalyze nucleotide release from heterotrimeric G-proteins has been also addressed by atomic-level simulations (Dror et al. 2015). The simulations indicated that the G-protein, even when it is not bound to the receptor, frequently adopts conformations that expose the guanosine diphosphate (GDP) nucleotide. Binding to the GPCR results in additional structural rearrangement that favors GDP release. In another work, the mechanism of receptor-mediated arrestin activation has been studied through extensive atomic-level simulations of arrestin (Latorraca et al. 2018). It was found that arrestin can be activated by binding to the GPCR core, the GPCR phosphorylated tail, or both. Molecular dynamics simulations were performed in conjunction with double electron–electron resonance (DEER) spectroscopy of activated rhodopsin in complex with the Gi protein to verify stability of the refined model (Huber and Sakmar 2008). The study revealed that Gi- and Gs-coupled GPCRs show different modes of G-protein binding. The Ras-like domain sits more upright on the receptor in the rhodopsin–Gi complex, and unlike the $\beta_2$AR–Gs structure, the C3 loop of rhodopsin makes contact with the $\beta$6-sheet of the Gi protein. Finally, a number of works have investigated the functional effect of dimerization (or oligomerization) of GPCRs, and have been thoroughly discussed along with experimental approaches in a recent review by Sakmar et al. (2017).

## Advanced Methods for Rhodopsin Molecular Simulations

### Gibbs Free Energy Calculations

At constant pressure and temperature, any isolated macrosystem tends to minimize its Gibbs free energy. For this reason, the Gibbs free energy surface, i.e., the Gibbs free energy as a function of coordinates, is one of the most fundamental properties in physics, chemistry, and biology (Jensen et al. 2014). For practical applications, usually only the difference in free energy between two states of a molecular system is calculated. For example, the Gibbs free energy difference between two rhodopsin conformations gives information about the relative concentrations of these two forms in equilibrium. The calculation of the Gibbs free energy difference between two states A and B is based on the general equation:

$$\Delta G = G_{\mathrm{B}} - G_{\mathrm{A}} = -k_{\mathrm{B}}T \ln \frac{Q_{\mathrm{B}}}{Q_{\mathrm{A}}}, \tag{3}$$

where $k_{\mathrm{B}}$ is the Boltzmann constant, $T$ is the temperature of the system, and $Q_i$ is the partition function for the system in the $i$th state. The partition function is described in terms of the Hamiltonian of the system:

$$Q_i = \frac{1}{h^3 N!} \int_{V_i} e^{-\frac{H_i(\mathbf{r},\mathbf{p})+PV}{k_{\mathrm{B}}T}} \mathrm{d}\mathbf{r}\mathrm{d}\mathbf{p}. \tag{4}$$

Here $V_i$ is the phase space of state $i$, $N$ is the number of atoms in the system, $h$ is Planck's constant, $H_i$ is the Hamiltonian of system, $\mathbf{r}$ represents the Cartesian coordinates of all atoms in the molecular system, $\mathbf{p}$ represents the conjugate momenta of all atoms, and $P$ and $V$ are the pressure and the volume of the system, respectively (Hansen and Van Gunsteren 2014). It has been shown that the term related with $PV$ is negligible, and it is not taken into account in actual calculations (Shirts and Mobley 2013). Below, we summarize the commonly applied computational approaches for the calculation of $\Delta G$, which is the Gibbs free energy difference.

### Free Energy Perturbation

The method of free energy perturbation is based on the Zwanzig relationship (Zwanzig 1954) that describes the $\Delta G$ between two nearby states of a molecular system, i.e., states with intersecting phase spaces:

$$\Delta G = -k_{\mathrm{B}}T \ln \left\langle e^{-\frac{\Delta U(\mathbf{r})}{k_{\mathrm{B}}T}} \right\rangle. \tag{5}$$

In the above formula, $\Delta U$ is the potential energy difference between the system in two close-lying states. Still, in most cases, the phase spaces of target states A and B do not intersect. The transformation from state $A$ to state $B$ can then be represented by a series of intermediate states, so that any neighboring pair of states along the path would have intersecting phase spaces. In this case, if the series of $N$ states is introduced, then $\Delta G$ can be calculated as

$$\Delta G = \sum_{i=1}^{N-1} \Delta G_{i,i+1}, \tag{6}$$

where $i = 1$ corresponds to state A, and $i = N$ corresponds to state B. Because $G$ is a state function of a system, any convenient path between A and B states can be constructed, and the intermediate states do not need to be physically realistic. The complete path can consist of several equilibrium end states connected by sub-paths of intermediate states, presented as a thermodynamic cycle.

As an example, consider the path for the retinal isomerization reaction in bovine visual rhodopsin (Fig. 6). Here, state A corresponds to dark-state rhodopsin that contains retinal in the 11-*cis* conformation, and state B corresponds

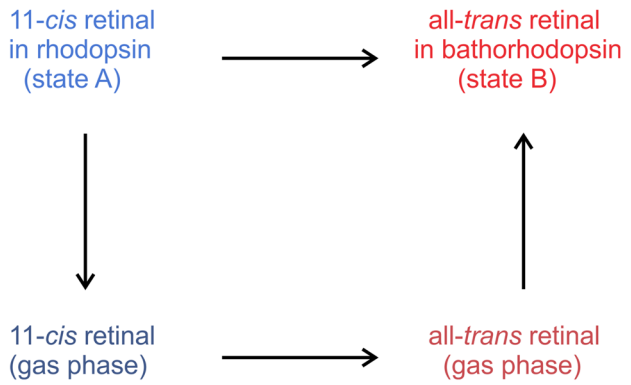


**Fig. 6** Example of thermodynamic cycle constructed for the calculation of difference in Gibbs free energy between bovine visual rhodopsin that contains 11-*cis* retinal and bathorhodopsin that contains all-*trans* retinal using the free-energy perturbation approach

to bathorhodopsin that contains all-*trans* retinal. The path consists of three transitions: transferring the 11-*cis* retinal from the gas phase to rhodopsin; the gas-phase transition between the 11-*cis* and all-*trans* retinal conformations, and transferring the all-*trans* retinal from the gas phase to bathorhodopsin. At each point, i.e., for each end state and for each intermediate state, equilibrium simulations are performed, and uncorrelated states (decoys) are extracted from the simulations. These decoys represent the ensemble of conformations for the specific state. Using the values of the potential energy for each conformation in the *i*th and $(i+1)$ th intermediate state, the $\Delta G_{i,i+1}$ difference can be calculated by applying Eq. (3).

For rhodopsins, free energy perturbation (FEP) has been applied for calculating the thermodynamic stability of water molecules located near the retinal protonated Schiff base in bacteriorhodopsin (Baudry et al. 2001; Roux et al. 1996). To accomplish this task, the free energy of transferring water molecules from the bulk phase to predefined sites inside protein cavities was calculated. In other studies, free energy perturbation was applied to calculate the binding affinities of different ligands to GPCRs, which is an essential step in rational drug design (Hénin et al. 2006; Lenselink et al. 2016).

## Thermodynamic Integration

The process of thermodynamic integration is closely related to the free energy perturbation approach. Here, the derivative $\mathrm{d}U/\mathrm{d}\lambda$ is calculated along the path between states *A* and *B*, where λ describes the distance variable (Shirts and Mobley 2013). The equation for calculating $\Delta G$ thus reads:

$$\Delta G = \int_0^1 \left\langle \frac{\mathrm{d}U(\mathbf{r},\lambda)}{\mathrm{d}\lambda} \right\rangle_\lambda \mathrm{d}\lambda, \tag{7}$$

where $\lambda = 0$ corresponds to the *A* state and $\lambda = 1$ corresponds to state *B*, and the angular brackets denote that the derivative is averaged over the ensemble. For rhodopsin, thermodynamic integration has been applied to compare the deprotonation free energy profiles of the retinal chromophore in the dark (11-*cis*) state of the bovine visual pigment and in its intermediate lumirhodopsin state. The study revealed the influence of the retinal orientation, hydrogen bonding network, and positioning of the protonated Schiff base counterion on the deprotonation efficiency (Van Keulen et al. 2017).

## Biased Molecular Dynamics Approaches

All the biased MD approaches are based on sampling of the actual trajectory between the equilibrium states A and B, and require knowledge of the reaction coordinate for the calculations. The reaction coordinate can be represented as a set of collective variables (CVs), which are the functions $\eta(\mathbf{r})$ of the Cartesian coordinates of the atoms constituting the molecular system. The motion of the CVs corresponds to the slow modes of the system dynamics that constitute the reaction process (Moradi et al. 2013). Examples of CVs are the isomerization angle, in the case of the C12–C13 = C14–C15 dihedral angle for the 13-*cis* to all-*trans* retinal isomerization of microbial rhodopsins, or the distance between the ligand and its interaction site for the binding reaction.

## Umbrella Sampling

The umbrella sampling (US) approach is based on calculation of the Landau free energy $G(\chi)$ along the reaction path:

$$G(\chi) = -k_\mathrm{B}TP(\chi), \tag{8}$$

where $\chi$ is the reaction coordinate, and $P(\chi)$ is the probability density function along the reaction coordinate. Thus, efficient sampling of all states along the A → B path is required. In the umbrella sampling approach, this requirement is achieved by introducing a bias potential (Kästner 2011). At each intermediate point ($\lambda_i$) along the path that crosses the free energy barrier, the system is sampled under the guidance of standard force field, with an extra term that constraints the system in the $\lambda_i$ vicinity. Usually, this extra term is represented by a harmonic function:

$$U_\mathrm{extra} = A(\chi - \chi_i)^2, \tag{9}$$

in which *A* is the constraint constant and $\chi_i$ is the value of the reaction coordinate at the $\lambda_i$ state. Afterward, a weighted histogram analysis (Kumar et al. 1992) is applied to derive the unbiased free energy along the path and, finally, the free energy difference between the A and B states. There are two key differences between umbrella sampling and the

free energy perturbation methodology. First, while during the FEP calculations an arbitrary path can be constructed between the A and B states, in the US approach the actual reaction coordinate should be used. Second, while during FEP calculations the system is fixed at the $\lambda_i$ points, in the US approach, the system is only constrained to move around $\lambda_i$ in a specific range.

For microbial rhodopsins, the umbrella sampling approach has been applied to investigate the retinal isomerization around the C13=C14 and C15=N bonds in bacteriorhodopsin. The difference in stability of the equilibrium (13,15)-*cis*, 13-*cis*-15-*trans*, 13-*trans*-15-*cis*, and all-*trans* conformations was thoroughly investigated, and allowed derivation of the entropy factor that stabilizes specific rhodopsin conformations (Baudry et al. 1997; Crouzy et al. 1999). In other studies, umbrella sampling was applied by Periole et al. (2012) to investigate the dimerization of visual rhodopsin, and to define the preferential dimerization interfaces.

### Metadynamics

For the calculation of $\Delta G$ values, metadynamics is representative of the adaptively biased molecular dynamics approaches that can be applied (Laio and Gervasio 2008; Moradi et al. 2013; Vymětal and Vondrášek 2010). Notably, in metadynamics sampling begins in one of the equilibrium states of the system (e.g., in the *A* state). During the simulation, an additional time-dependent biasing potential is added to the equations of motion. This biasing potential adds potential energy to the collective variables, so that the movement of the system along the reaction coordinate becomes more pronounced. Usually, symmetric biasing potentials, e.g., those based on B-splines (Laio and Parrinello 2002; Moradi et al. 2013), are applied. During the simulation, the free energy barrier between A and B states becomes flat, and the system starts moving freely along the reaction path. In the long-time limit, the free energy along the reaction path can be derived as:

$$G(\chi) = -V_{\text{bias}}(\chi) + C, \tag{10}$$

where $C$ is a constant and $V_{\text{bias}}(\chi)$ is the added bias potential. Although adding biased potentials of fixed height can lead to overfilling of the free energy surface along the reaction path, well-tempered metadynamics that introduces biased potentials which steadily diminish with time can be applied to overcome this problem (Barducci et al. 2008). Modern developments of metadynamics algorithms are connected to the application of replica-exchange during the simulations. In multiple-walkers metadynamics, several simulations are run in parallel, each with its specific biasing potential and temperature of simulation (Raiteri et al. 2006). The rules for the exchange of states between trajectories are usually based on the Metropolis criterion (Metropolis and Ulam 1949).

In this way, metadynamics has been applied to investigate the free energy differences between metastable states that emerge during the photosequence of bovine rhodopsin (Provasi et al. 2009). Also, the free energy landscape between the photoactivated deprotonated bovine rhodopsin and the low-pH ground state of 11-*cis*-retinylidene rhodopsin in the presence of the lipid membrane environment has been investigated (Provasi and Filizola 2010). Two additional studies aimed at the investigation of the channelrhodopsin-2 proton pump have applied metadynamics for deriving important information about the protein functioning. In the first work, metadynamics allowed the performance of extensive sampling of retinal isomerization in channelrhodopsin-2. The free energy profile of the isomerization process was derived, and the water penetration through the protein pore was sampled during the protein isomerization (Ardevol and Hummer 2018). In the second work, well-tempered metadynamics was applied to investigate the reorientation of the Glu123 counterion of the retinylidene protonated Schiff base in channelrhodopsin-2. Here, the dependence of the free energy value on the Glu123 orientation angle was calculated for the wild-type protein and its C128T mutant which demonstrates substantially different photocycle kinetics (Guo et al. 2016). In other studies metadynamics was applied to investigate the activation processes, and the possible metastable states of other classes of GPCRs (Gushchin et al. 2013; Meral et al. 2018), or to evaluate the binding affinities of ligands to GPCRs (Saleh et al. 2017). Metadynamics has also been combined with the umbrella sampling approach to investigate the relative stability of dimer interfaces in human $\beta$-adrenergic receptors, which required the introduction of several angle-related and distance-related collective variables (Johnston et al. 2012). During the metadynamics simulation, the bias potential was added only to the distance-related collective variable, generating the starting states for umbrella sampling simulations of the angle-related collective variables.

### Steered Molecular Dynamics

Another approach for practical calculation of the free energy difference between the states is based on the Jarzynski equation. As shown by Jarzynski (1997) the $\Delta G$ between states A and B can be evaluated as:

$$\Delta G \approx -k_{\text{B}}T \ln \left\langle e^{-\frac{W}{k_{\text{B}}T}} \right\rangle, \tag{11}$$

where $W$ is the work that is required to pull the system from state A to state B. To apply the Jarzynski equation, sampling of the steered molecular dynamics (SMD) simulation is required. In SMD, an artificial force is applied that pulls the system from state A (e.g., unbound protein–ligand system)

to state B (bound protein–ligand system), and several A → B and B → A simulations are sampled.

The SMD-based approach for free energy calculation was applied to study the energy profile of sodium ion translocation through the pore of the sodium-pumping microbial rhodopsin KR2 (Suomivuori et al. 2017). For microbial rhodopsins, SMD per se was applied to investigate the torsion of specific alpha helices during the primary events after photoactivation (Saam et al. 2002), the process of retinal binding in bacteriorhodopsin (Isralewitz et al. 1997), and the process of sodium ion conduction through channelrhodopsin-2 (Richards and Dempski 2017). In addition, this approach has been applied to evaluate the binding affinities of different ligands to GPCRs, e.g., the $\beta$-adrenergic receptors (González et al. 2011).

### Coarse-Grained Molecular Dynamics Simulations

Coarse-grained (CG) simulations are applied when the long time-scale dynamics of the system are required for the investigation of the target process (e.g., conformational changes of a membrane-protein complex), while the atomistic precision is either less essential (Noid 2013), or incorporated by a multiscale modeling approach as pioneered by Voth et al. (Ayton et al. 2007; Izvekov and Voth 2005; Saunders and Voth 2013). However, if the process under study is more complex and requires higher precision, then a hybrid MM/CG approach (that is described in the "Hybrid Molecular Mechanics/Coarse-Grained Simulations" section) is applied (Leguèbe et al. 2012). To reduce the computational cost of simulations, i.e., to reduce the dimensionality of the simulated molecular system, in the CG approach the groups of atoms are combined into interaction sites with specific physical and chemical properties. The strong requirement is that each atom can be a part of only one interaction site (Noid 2013). Usually, each interaction site consists of 2–10 "heavy" atoms with associated hydrogen atoms. Besides the reduction of dimensionality, the CG simulations do not include fast movements (such as vibrations of C–H bonds), and for this reason they allow an increase in the time step of the MD simulations (Marrink et al. 2004; Noid 2013). Moreover, the averaging in the CG simulations leads to the implicit inclusion of entropic effects, thereby increasing the speed of the conformational space investigation. Several force fields have been developed for CG simulations, among which the MARTINI force field of Marrink et al. (2007) is the most commonly applied. The MARTINI force field maps four "heavy" atoms to one interaction site, with the exception of ring moieties, for which two "heavy" atoms correspond to one interaction site. The functional form of the MARTINI force field is the same as the form of standard atomistic force fields, such as AMBER or CHARMM (Klauda et al. 2010; Lindorff-Larsen et al. 2010). The CG force field must obey specific consistency conditions, i.e., the structural and thermodynamic properties of the system during the MD simulation under the guidance of the atomistic and CG force fields should be similar. For example, the parameterization of nonbonded interactions during the development of the MARTINI force field involved comparing the calculated thermodynamic properties, such as hydration and vaporization free energies (Monticelli et al. 2008), with the experimental values. For parameterization of bonded interactions, the reproducibility of structural features was evaluated.

The CG approach has been applied in a large number of studies of visual and microbial rhodopsins. For example, it was used to study the adaptation of the lipid membrane structure in the vicinity of visual rhodopsin (Periole et al. 2007), which required running 8-$\mu$s MD simulations for the proteolipid membrane system. In other studies, the CG MD simulations were applied to define the cholesterol binding sites at the rhodopsin surface, to derive energy profiles for lipid–rhodopsin interactions (Horn et al. 2014; Periole 2016; Scott et al. 2008), and to investigate the assembly of lipid nanodisks around microbial rhodopsins (Sahoo et al. 2019). Furthermore, CG MD simulations have been used to investigate long-lasting processes in rhodopsins, e.g., modeling of the complete bacteriorhodopsin photocycle (Tavanti and Tozzini 2014), the unfolding of bacteriorhodopsin in the membrane (Yamada et al. 2016), and the adaptation of visual rhodopsin to a lipidic cubic phase environment (Khelashvili et al. 2012). An approach involving CG MD simulations in combination with normal mode analysis was also used to study the allosteric regulation, i.e., the structural determinants that regulate ligand binding in visual rhodopsin and other GPCRs (Balabin et al. 2009).

## Quantum Mechanics/Molecular Mechanics Models

In a QM/MM model, the system is divided into two subsystems: the molecular mechanics (MM) and quantum mechanics (QM) parts. There are two approaches to deal with the model: a subtractive scheme and an additive scheme. In the subtractive scheme (Svensson et al. 1996; Vreven and Morokuma 2006), the QM/MM energy of the system is given by:

$$V_{\mathrm{QM/MM}} = V_{\mathrm{MM}}(\mathrm{QM}+\mathrm{MM}) + V_{\mathrm{QM}}(\mathrm{QM}) - V_{\mathrm{MM}}(\mathrm{QM}). \tag{12}$$

Here, $V_{MM}(QM+MM)$ is the energy of the whole system calculated at the MM level, $V_{QM}(QM)$ is the energy of the QM subsystem calculated at the QM level, and finally, $V_{MM}(QM)$ is the energy of the QM subsystem calculated at the MM level.

In additive schemes (Field et al. 1990), the QM part is embedded within the MM system, and the total potential energy is represented as a sum of the QM energy term, the MM energy term, and the QM/MM coupling term:

$$V_{\mathrm{QM/MM}} = V_{\mathrm{QM}}(\mathrm{QM}) + V_{\mathrm{MM}}(\mathrm{MM}) + V_{\mathrm{QM/MM}}. \quad (13)$$

The molecular mechanics force fields are described above. To treat the QM part, which is usually a Schiff base in rhodopsins, both ab initio and density functional theory (DFT) methodologies are applied. The choice of the QM methodology is dictated by the problem. For example, to treat the spectral properties, multiconfigurational and multireference methods, such as CASPT2 (Finley et al. 1998), MRCI (Lischka et al. 2002), SORCI (Nikolaev et al. 2017; Ryazantsev et al. 2012), or analogs are applied. For description of the ground state, usually a DFT (Elstner et al. 2003) or SCC-DFTB (Elstner 2006; Gaus et al. 2011) calculation, which is a semiempirical variation of DFT, is a method of choice.

## Treatment of Electronic Structure of Retinal Chromophore

The ability of QM/MM methodologies to treat the electronic structure of the retinal chromophore placed in the protein environment makes this approach a method of choice for studying the optical and photochemical properties of rhodopsins. In a number of studies, the effect of the protein environment, including both steric and electrostatic interactions, on the retinal structure and optical properties, has been investigated (Altun et al. 2008b; Andruniów et al. 2004; Bravaya et al. 2007; Coto et al. 2006a; 2008; Gozem et al. 2017; Hoffmann et al. 2006). For microbial rhodopsins, the electrostatic interactions of the retinal chromophore with polar and charged residues of the protein play a major role in spectral color tuning, while steric interactions usually provide a negligible effect (Hoffmann et al. 2006; Ryazantsev et al. 2012). For visual rhodopsins, the effect caused by the retinal deformation is more pronounced, but the electrostatic interaction still plays the major role (Altun et al. 2008b). Among all the charged residues, the negatively charged counterion residue, which is located in the retinal-binding pocket of the rhodopsin proteins in the vicinity of the $N–H^+$ moiety, is the most important, causing a large blue shift of the absorption maxima from its gas phase value, 610 nm and 615 nm for 11-*cis* and all-*trans* protonated Schiff bases, respectively (Nielsen et al. 2006). The rest of the protein either enhances this blue shift, or provides the redshift that partially compensates the effect of the counterion (Altun et al. 2008a; Hoffmann et al. 2006; Nikolaev et al. 2019a; Rajamani and Gao 2002; Ryazantsev et al. 2012).

The important role of charged and polar residues in color tuning was demonstrated in bovine rhodopsin (Altun et al. 2008a; b; Bravaya et al. 2007; Coto et al. 2006b), halorhodopsins (Ryazantsev et al. 2012), bacteriorhodopsin (Rajamani and Gao 2002), visual cone pigments (Frähmcke et al. 2012; Fujimoto et al. 2006; Zhou et al. 2014), mutants of *Anabaena* sensory rhodopsin (Melaccio et al. 2012), intermediates of the rhodopsin photocycle (Campomanes et al. 2014), the deprotonated M state of bacteriorhodopsin (Fujimoto et al. 2010), and blue-light absorbing proteorhodopsin (Hillebrecht et al. 2006). For example, Fujimoto et al. (2005) and Hoffman et al. (2006) considered the spectral shift between bacteriorhodopsin and sensory rhodopsin-II. It was demonstrated that the major part of the spectral shift was provided by the differences in the positions of the negatively charged counterions and in the orientations of polar residues (Hoffmann et al. 2006). The importance of protein reorganization in the color-tuning mechanism was also demonstrated for the chloride-bound and anion-free halorhodopsins (Ryazantsev et al. 2012). Here, the authors demonstrated that the 22-nm blue shift that is observed upon chloride binding in the *N. pharaonis* halorhodopsin consists of two terms: a 95-nm blue shift induced by a negatively charged chloride ion and a 73-nm red shift caused by the protein reorganization. In a number of studies, absorption maxima calculations along with energy calculations were applied to define the protonation state of the Glu181 residue in bovine rhodopsin (Frähmcke et al. 2010; Hall et al. 2008). Unfortunately, the results could not be interpreted unambiguously, partially because of the relatively large distance between the Glu181 residue and the retinal chromophore in bovine rhodopsin.

## Photoisomerization of the Retinal Cofactor

In other QM/MM studies, the photochemical step of the rhodopsin photocycle, i.e., the isomerization of the retinal chromophore in the protein environment, has been investigated (Curchod and Martínez 2018; Gozem et al. 2017). Upon absorption of a photon, the retinal chromophore is excited from the ground state (S0) to the first excited singlet state (S1). Thereafter, the S1 state evolves from the Frank–Condon (FC) region of the S1 potential energy surface (PES) toward the conical intersection (CI)—the region where the PES of the S1 and S0 states intersect. From the CI point, the system can evolve either into the product state (the isomerized state), or back to the reactant state. One of the unique features of the rhodopsin proteins is that the photoactivated isomerization is performed with a high quantum yield and at the ultrafast time scale, especially when compared to the retinal isomerization in methanol solution (Andruniów et al. 2004; Frutos et al. 2007; Khrenova et al. 2010; Kukura et al. 2005; Schapiro et al. 2008, 2011;

Schnedermann et al. 2018; Schoenlein et al. 1991; Wang et al. 1994). It has been postulated that the electrostatic field produced by the rhodopsin environment catalyzes the retinal isomerization process (Andruniów et al. 2004; Schapiro et al. 2011; Tomasello et al. 2009). To obtain the atomistic details of the retinal isomerization, the evolution of the excited state on the S1 PES has to be simulated from the FC region to the CI point. Here, two approaches have been applied: static calculation of the S1 PES topology, and direct on-the-fly dynamics starting from Franck–Condon points going to the products.

(*i*) Investigation of the important topological features of the potential energy surface includes minima, transition states, conical intersections, and minimal energy paths. In several works, the minimal energy path (MEP) on the S1 potential has been calculated (Coto et al. 2006a, 2008; El-Khoury et al. 2009; González-Luque et al. 2000; Sumita et al. 2009). Generally, the MEP provides the insight into the topology of the S1 PES, and allows for defining intermediate states of the retinal isomerization. Other studies have concentrated directly on the geometry and energetics of the retinal chromophore in the critical CI point (Coto et al. 2006a). It has been shown that the isomerization angle (C11=C12 torsional angle for visual rhodopsin and C13=C14 torsional angle for microbial rhodopsins) is twisted by 90° at the CI point.

(*ii*) Evolution of the excited state from the FC region toward the CI point is provided by QM/MM MD simulations (Andruniów et al. 2004; Frutos et al. 2007; Khrenova et al. 2010; Schapiro et al. 2008, 2011). Using this method, researchers have distinguished the three major motions (modes) that are involved in the retinal isomerization: torsional deformation of the reactive bond, bond length alteration (BLA), and the hydrogen-out-of-plane (HOOP) mode. The BLA mode represents the stretching vibration of the bonds along the main chain of the retinal, and leads to the inversion of single and double bonds. The HOOP mode represents the wagging motion of the hydrogens bound to the carbon atoms that constitute the reactive double bond. Notably, the HOOP motion greatly accelerates the isomerization process. The majority of studies have concentrated on the retinal isomerization in bovine visual rhodopsin; however, similar QM/MM MD trajectories were also calculated for isorhodopsin (bovine rhodopsin containing 9-*cis* retinal) (Chung et al. 2012; Strambi et al. 2008), nonvisual human melanopsin (Rinaldi et al. 2014), and bacteriorhodopsin (Li et al. 2011; Warshel and Chu 2001). For example, Chung et al. (2012) showed that while in bovine rhodopsin retinal undergoes a straightforward isomerization directly into the all-*trans* state (bathorhodopsin), isorhodopsin demonstrates a more complex isomerization path that branches in two possible directions.

### Polarizability and Charge-Transfer Effects

Finally, a number of studies concentrated on the extension of QM/MM methodology to take into account polarizability and charge transfer effects in the retinal binding pocket (Caprasecca et al. 2014; Söderhjelm et al. 2009; Wanko et al. 2008a, b). Here, two approaches were applied. In the first approach, a part of the retinal binding pocket was included in the QM part at a lower level of theory (QM/QM/MM approach). Using this methodology, Wanko et al. (2008b) demonstrated that polarizability and charge transfer effects lead to a 0.08–0.09 eV bathochromic shift of the absorption maxima. In the second approach, the effect of polarization was taken into account by applying a polarizable MM force field for the opsin environment (Caprasecca et al. 2014), while QM calculations were performed only for the retinal chromophore.

### QM/MM Free Energy Optimization of Retinal Chromophore in the Protein Environment

Because molecular systems tend to a minimum of the Gibbs free energy, the minimization of this function rather than the potential energy is preferred during geometry optimization. Such optimization is based on the calculation of free energy gradients (FEG) as proposed by Okuyama-Yoshida et al. (2000), and is applied to optimize the target molecule at the QM level, in the environment described at the MM level. During minimization, the force acting on the atoms of QM subsystem can be calculated through the following relationship:

$$F(\mathbf{r}) = -\frac{\partial G(\mathbf{r})}{\partial \mathbf{r}} \approx -\frac{\partial \langle U \rangle}{\partial \mathbf{r}}, \tag{14}$$

where $\mathbf{r}$ represents the Cartesian coordinates of the optimized QM subsystem, $G$ is the Gibbs free energy of the system and $\langle U \rangle$ is the average potential energy of the QM subsystem that includes its interaction with the environment. To calculate the average potential energy, two approaches have been proposed. In the first approach, called ASEP (average solvent electrostatic potential), the average interaction between the QM subsystem and the MM environment is calculated (Galván et al. 2003). In the second approach, referred to as ASEC (average solvent electrostatic configuration), the QM subsystem is optimized in the modified environment presented as an ensemble of noncorrelated environment configurations (Coutinho et al. 2007). Recently, this approach was applied to optimize the retinal chromophore in the rhodopsin environment (Orozco-Gonzalez et al. 2017). To generate the ensemble of configurations, a preliminary MD trajectory was simulated, and $N$ uncorrelated configurations (decoys) were extracted from the trajectory. Thereafter,

all the *N* decoys were superimposed to construct the average environment (consisting of *NM* virtual atoms, where *M* is the number of atoms in the MM subsystem). To conserve the interaction forces, the nonbonded interactions between the QM subsystem and the MM environment were properly scaled. Each virtual atom of the new MM environment had a charge that was *N* times smaller than the charge of the corresponding atom in the actual protein. The terms that describe the van der Waals interactions were also decreased *N* times. After the generation of the average environment, the QM/MM optimization of the retinal chromophore was performed.

### Hybrid Molecular Mechanics/Coarse-Grained Simulations

The investigation of certain processes may require long simulation times of large molecular systems (e.g., membrane-embedded rhodopsin) on one hand, and the atomistic description of the target process on the other hand. To overcome this problem, the hybrid MM/CG approach can be applied (Leguèbe et al. 2012). Here, the system is represented at an atomistic level, i.e., its dynamics are calculated by utilizing an atomistic MM force field, and the rest of the system is modeled at the CG level, under the guidance of the CG force field. To our knowledge, the MM/CG approach has not yet been applied to investigate rhodopsins; however, it has been implemented for other GPCRs. Examples include ligand binding to the TAS2R38 bitter taste receptor (Marchiori et al. 2013) and the $\beta$-adrenergic receptors (Leguèbe et al. 2012). In both cases, the ligand and its binding site were sampled at the atomistic MM level, while the rest of GPCR and the membrane environment were sampled at the CG level.

## Conclusions

In this article, we reviewed the modern computational methodologies used for modeling rhodopsin dynamics and the properties at different time scales and levels of precision. Due to the further development of both computational methodologies and the performance of computer systems, the role of computational modeling in understanding and predicting rhodopsin properties will be steadily increasing. First, the accuracy of applied computational models can be improved. Second, as described above, computational studies of rhodopsins require extensive MM and QM/MM sampling, which is becoming possible due to increasing availability of the high-performance calculations, including massively parallel calculations on graphics processors units. When prediction of rhodopsin structure is concerned, the explicit inclusion of the retinal chromophore and the implicit inclusion of the membrane environment can increase the quality of predicted models. Other improvements of the model construction are related with the increasing accuracy of water prediction, and with applying p$K_A$ calculations "on the fly" during the MD sampling. Precise prediction of water locations in critical cases can be related with the application of MM-based free energy estimation approaches, such as free energy perturbation. For the p$K_A$ calculations, application of constant-pH MD approaches during sampling should be considered. Finally, development of improved force fields for the retinal chromophore is directly related with the increase of accuracy in MM calculations. These new force fields should take polarization and charge-transfer effects into account, better treat the van der Waals interactions, and also should be easily integrated in the standard MM force fields for proteins, such as AMBER or CHARMM. Future development of such force fields should apply modern machine learning techniques that utilize data from QM/MM MD simulations to derive more accurate parameters.

**Funding** This work was supported by the US National Institutes of Health (EY012049 and EY02604) and by the US National Science Foundation (MCB 1817862 and CHE 1904125) (to M.F.B.). A.V.S. was supported by the Russian Foundation for Basic Research (Grant 16-04-00494A). M.N.R. was supported by the Skolkovo Foundation (Grant agreement for Russian educational and scientific organization No. 7 dd 19.12.2017) and the Skolkovo Institute of Science and Technology (General agreement No. 3663-MRA dd 25.12.2017).

### Compliance with Ethical Standards

**Conflict of interest** The authors declare that they have no conflicts of interest.

**Research Involving Human and Animal Participants** This article does not contain any studies with human participants or animals performed by any of the authors.

## References

Ahuja S, Crocker E, Eilers M, Hornak V, Hirshfeld A, Ziliox M, Syrett N, Reeves PJ, Khorana HG, Sheves M, Smith SO (2009a) Location of the retinal chromophore in the activated state of rhodopsin. J Biol Chem 284:10190–10201

Ahuja S, Hornak V, Yan EC, Syrett N, Goncalves JA, Hirshfeld A, Ziliox M, Sakmar TP, Sheves M, Reeves PJ, Smith SO, Eilers M (2009b) Helix movement is coupled to displacement of the second extracellular loop in rhodopsin activation. Nat Struct Mol Biol 16:168–175

Alford RF, Leaver-Fay A, Jeliazkov JR, O'Meara MJ, DiMaio FP, Park H, Shapovalov MV, Renfrew PD, Mulligan VK, Kappel K, Labonte JW, Pacella MS, Bonneau R, Bradley P, Dunbrack RL Jr, Das R, Baker D, Kuhlman B, Kortemme T, Gray JJ (2017) The Rosetta all-atom energy function for macromolecular modeling and design. J Chem Theory Comput 13:3031–3048

Altun A, Yokoyama S, Morokuma K (2008a) Mechanism of spectral tuning going from retinal in vacuo to bovine rhodopsin and its mutants: multireference ab initio quantum mechanics/molecular mechanics studies. J Phys Chem B 112:16883–16890

Altun A, Yokoyama S, Morokuma K (2008b) Spectral tuning in visual pigments: an ONIOM (QM: MM) study on bovine rhodopsin and its mutants. J Phys Chem B 112:6814–6827

Amora TL, Ramos LS, Galan JF, Birge RR (2008) Spectral tuning of deep red cone pigments. Biochemistry 47:4614–4620

Andruniów T, Ferré N, Olivucci M (2004) Structure, initial excited-state relaxation, and energy storage of rhodopsin resolved at the multiconfigurational perturbation theory level. Proc Natl Acad Sci USA 101:17908–17913

Ardevol A, Hummer G (2018) Retinal isomerization and water-pore formation in channelrhodopsin-2. Proc Natl Acad Sci USA 115:3557–3562

Ayton GS, Noid WG, Voth GA (2007) Multiscale modeling of biomolecular systems: in serial and in parallel. Curr Opin Struct Biol 17:192–198

Balabin IA, Yang W, Beratan DN (2009) Coarse-grained modeling of allosteric regulation in protein receptors. Proc Natl Acad Sci USA 106:14253–14258

Barducci A, Bussi G, Parrinello M (2008) Well-tempered metadynamics: a smoothly converging and tunable free-energy method. Phys Rev Lett 100:020603

Baudry J, Crouzy S, Roux B, Smith JC (1997) Quantum chemical and free energy simulation analysis of retinal conformational energetics. J Chem Inf Comput Sci 37:1018–1024

Baudry J, Crouzy S, Roux B, Smith JC (1999) Simulation analysis of the retinal conformational equilibrium in dark-adapted bacteriorhodopsin. Biophys J 76:1909–1917

Baudry J, Tajkhorshid E, Molnar F, Phillips J, Schulten K (2001) Molecular dynamics study of bacteriorhodopsin and the purple membrane. J Phys Chem B 105:905–918

Bondar A-N, Knapp-Mohammady M, Suhai S, Fischer S, Smith JC (2011) Ground-state properties of the retinal molecule: from quantum mechanical to classical mechanical computations of retinal proteins. Theoret Chem Acc 130:1169–1183

Bravaya K, Bochenkova A, Granovsky A, Nemukhin A (2007) An opsin shift in rhodopsin: retinal S0–S1 excitation in protein, in solution, and in the gas phase. J Am Chem Soc 129:13035–13042

Brown MF (1994) Modulation of rhodopsin function by properties of the membrane bilayer. Chem Phys Lipids 73:159–180

Brown MF (2012) Curvature forces in membrane lipid–protein interactions. Biochemistry 51:9782–9795

Brown MF (2017) Soft matter in lipid–protein interactions. Ann Rev Biophys 46:379–410

Campomanes P, Neri M, Horta BA, Röhrig UF, Vanni S, Tavernelli I, Rothlisberger U (2014) Origin of the spectral shifts among the early intermediates of the rhodopsin photocycle. J Am Chem Soc 136:3842–3851

Caprasecca S, Jurinovich S, Viani L, Curutchet C, Mennucci B (2014) Geometry optimization in polarizable QM/MM models: the induced dipole formulation. J Chem Theory Comput 10:1588–1598

Chen J, Hundertmark D, Martínez TJ (2008) A unified theoretical framework for fluctuating-charge models in atom-space and in bond-space. J Chem Phys 129:214113

Chen H-F, Inoue K, Ono H, Abe-Yoshizumi R, Wada A, Kandori H (2018) Time-resolved FTIR study of light-driven sodium pump rhodopsins. Phys Chem Chem Phys 20:17694–17704

Choe H-W, Kim YJ, Park JH, Morizumi T, Pai EF, Krauss N, Hofmann KP, Scheerer P, Ernst OP (2011) Crystal structure of metarhodopsin II. Nature 471:651–655

Chothia C, Lesk AM (1986) The relation between the divergence of sequence and structure in proteins. EMBO J 5:823–826

Chung WC, Nanbu S, Ishida T (2012) QM/MM trajectory surface hopping approach to photoisomerization of rhodopsin and isorhodopsin: the origin of faster and more efficient isomerization for rhodopsin. J Phys Chem B 116:8009–8023

Chung LW, Sameera WMC, Ramozzi R, Page AJ, Hatanaka M, Petrova GP, Harris TV, Li X, Ke Z, Liu F, Li H-B, Ding L, Morokuma K (2015) The ONIOM method and its applications. Chem Rev 115:5678–5796

Cordomí A, Caltabiano G, Pardo L (2012) Membrane protein simulations using AMBER force field and Berger lipid parameters. J Chem Theory Comput 8:948–958

Cornell WD, Cieplak P, Bayly CI, Gould IR, Merz KM, Ferguson DM, Spellmeyer DC, Fox T, Caldwell JW, Kollman PA (1995) A second generation force field for the simulation of proteins, nucleic acids, and organic molecules. J Am Chem Soc 117:5179–5197

Coto PB, Sinicropi A, De Vico L, Ferré N, Olivucci M (2006a) Characterization of the conical intersection of the visual pigment rhodopsin at the CASPT2//CASSCF/AMBER level of theory. Mol Phys 104:983–991

Coto PB, Strambi A, Ferré N, Olivucci M (2006b) The color of rhodopsins at the ab initio multiconfigurational perturbation theory resolution. Proc Natl Acad Sci USA 103:17154–17159

Coto PB, Strambi A, Olivucci M (2008) Effect of opsin on the shape of the potential energy surfaces at the conical intersection of the rhodopsin chromophore. Chem Phys 347:483–491

Coutinho K, Georg H, Fonseca T, Ludwig V, Canuto S (2007) An efficient statistically converged average configuration for solvent effects. Chem Phys Lett 437:148–152

Crouzy S, Baudry J, Smith JC, Roux B (1999) Efficient calculation of two-dimensional adiabatic and free energy maps: application to the isomerization of the C13–C14 and C15–N16 bonds in the retinal of bacteriorhodopsin. J Comput Chem 20:1644–1658

Crozier PS, Stevens MJ, Forrest LR, Woolf TB (2003) Molecular dynamics simulation of dark-adapted rhodopsin in an explicit membrane bilayer: coupling between local retinal and larger scale conformational change. J Mol Biol 333:493–514

Curchod BF, Martínez TJ (2018) Ab initio nonadiabatic quantum molecular dynamics. Chem Rev 118:3305–3336

De Groot HJ, Smith SO, Courtin J, Van den Berg E, Winkel C, Lugtenburg J, Griffin RG, Herzfeld J (1990) Solid-state carbon-13 and nitrogen-15 NMR study of the low pH forms of bacteriorhodopsin. Biochemistry 29:6873–6883

Deupi X, Edwards P, Singhal A, Nickle B, Oprian D, Schertler G, Standfuss J (2012) Stabilized G protein binding site in the structure of constitutively active metarhodopsin-II. Proc Natl Acad Sci USA 109:119–124

Dickson CJ, Madej BD, Skjevik ÅA, Betz RM, Teigen K, Gould IR, Walker RC (2014) Lipid14: the Amber lipid force field. J Chem Theory Comput 10:865–879

Doemer M, Maurer P, Campomanes P, Tavernelli I, Rothlisberger U (2013) Generalized QM/MM force matching approach applied to the 11-*cis* protonated Schiff base chromophore of rhodopsin. J Chem Theory Comput 10:412–422

Dolinsky TJ, Nielsen JE, McCammon JA, Baker NA (2004) PDB2PQR: an automated pipeline for the setup of Poisson-Boltzmann electrostatics calculations. Nucleic Acids Res 32:W665–W667

Dolinsky TJ, Czodrowski P, Li H, Nielsen JE, Jensen JH, Klebe G, Baker NA (2007) PDB2PQR: expanding and upgrading automated preparation of biomolecular structures for molecular simulations. Nucleic Acids Res 35:W522–W525

Dorn M, de Silva MB, Buriol LS, Lamb LC (2014) Three-dimensional protein structure prediction: methods and computational strategies. Comput Biol Chem 53:251–276

Dror RO, Arlow DH, Borhani DW, Jensen MØ, Piana S, Shaw DE (2009) Identification of two distinct inactive conformations of

the $\beta_2$-adrenergic receptor reconciles structural and biochemical observations. Proc Natl Acad Sci USA 106:4689–4694
Dror RO, Arlow DH, Maragakis P, Mildorf TJ, Pan AC, Xu H, Borhani DW, Shaw DE (2011) Activation mechanism of the $\beta_2$-adrenergic receptor. Proc Natl Acad Sci USA 108:18684–18689
Dror RO, Green HF, Valant C, Borhani DW, Valcourt JR, Pan AC, Arlow DH, Canals M, Lane JR, Rahmani R, Baell JB, Sexton PM, Christopoulos A, Shaw DE (2013) Structural basis for modulation of a G-protein-coupled receptor by allosteric drugs. Nature 503:295–299
Dror RO, Mildorf TJ, Hilger D, Manglik A, Borhani DW, Arlow DH, Philippsen A, Villanueva N, Yang Z, Lerch MT, Hubbell WL, Kobilka BK, Sunahara RK, Shaw DE (2015) Structural basis for nucleotide exchange in heterotrimeric G proteins. Science 348:1361–1365
Ebejer J-P, Hill JR, Kelm S, Shi J, Deane CM (2013) Memoir: template-based structure prediction for membrane proteins. Nucleic Acids Res 41:W379–W383
El-Khoury PZ, Tarnovsky AN, Schapiro I, Ryazantsev MN, Olivucci M (2009) Structure of the photochemical reaction path populated via promotion of $CF_2I_2$ into its first excited state. J Phys Chem A 113:10767–10771
Elstner M (2006) The SCC-DFTB method and its application to biological systems. Theoret Chem Acc 116:316–325
Elstner M, Frauenheim T, Suhai S (2003) An approximate DFT method for QM/MM simulations of biological structures and processes. J Mol Struct (Theochem) 632:29–41
Eswar N, Webb B, Marti-Renom MA, Madhusudhan MS, Eramian D, Shen M-y, Pieper U, Sali A (2006) Comparative protein structure modeling using Modeller. Curr Protoc Bioinf 15:5.6.1–5.6.30
Feig M (2008) Implicit membrane models for membrane protein simulation. Methods Mol Biol 443:181–196
Feller SE, Gawrisch K, Woolf TB (2003) Rhodopsin exhibits a preference for solvation by polyunsaturated docosohexaenoic acid. J Am Chem Soc 125:4434–4435
Feng J, Brown MF, Mertz B (2015) Retinal flip in rhodopsin activation? Biophys J 108:2767–2770
Ferrand M, Zaccai G, Nina M, Smith J, Etchebest C, Roux B (1993) Structure and dynamics of bacteriorhodopsin: comparison of simulation and experiment. FEBS Lett 327:256–260
Field MJ, Bash PA, Karplus M (1990) A combined quantum mechanical and molecular mechanical potential for molecular dynamics simulations. J Comput Chem 11:700–733
Finley J, Malmqvist P-Å, Roos BO, Serrano-Andrés L (1998) The multi-state CASPT2 method. Chem Phys Lett 288:299–306
Fracchia F, Del Frate G, Mancini G, Rocchia W, Barone V (2017) Force field parametrization of metal ions from statistical learning techniques. J Chem Theory Comput 14:255–273
Frähmcke JS, Wanko M, Phatak P, Mroginski MA, Elstner M (2010) The protonation state of Glu181 in rhodopsin revisited: interpretation of experimental data on the basis of QM/MM calculations. J Phys Chem B 114:11338–11352
Frähmcke JS, Wanko M, Elstner M (2012) Building a model of the blue cone pigment based on the wild type rhodopsin structure with QM/MM methods. J Phys Chem B 116:3313–3321
Frutos LM, Andruniów T, Santoro F, Ferré N, Olivucci M (2007) Tracking the excited-state time evolution of the visual pigment with multiconfigurational quantum chemistry. Proc Natl Acad Sci USA 104:7764–7769
Fujimoto K, Hasegawa J-y, Hayashi S, Kato S, Nakatsuji H (2005) Mechanism of color tuning in retinal protein: SAC-CI and QM/MM study. Chem Phys Lett 414:239–242
Fujimoto K, Hasegawa J-y, Hayashi S, Nakatsuji H (2006) On the color-tuning mechanism of Human-Blue visual pigment: SAC-CI and QM/MM study. Chem Phys Lett 432:252–256
Fujimoto KJ, Asai K, Hasegawa J-y (2010) Theoretical study of the opsin shift of deprotonated retinal Schiff base in the M state of bacteriorhodopsin. Phys Chem Chem Phys 12:13107–13116
Galván IF, Sánchez M, Martín M, Olivares del Valle F, Aguilar M (2003) Geometry optimization of molecules in solution: joint use of the mean field approximation and the free-energy gradient method. J Chem Phys 118:255–263
Gasteiger J, Marsili M (1980) Iterative partial equalization of orbital electronegativity—a rapid access to atomic charges. Tetrahedron 36:3219–3228
Gaus M, Cui Q, Elstner M (2011) DFTB3: extension of the self-consistent-charge density-functional tight-binding method (SCC-DFTB). J Chem Theory Comput 7:931–948
Gellini C, Lüttenberg B, Sydor J, Engelhard M, Hildebrandt P (2000) Resonance Raman spectroscopy of sensory rhodopsin II from *Natronobacterium pharaonis*. FEBS Lett 472:263–266
González A, Perez-Acle T, Pardo L, Deupi X (2011) Molecular basis of ligand dissociation in $\beta$-adrenergic receptors. PLoS ONE 6:e23815
González-Luque R, Garavelli M, Bernardi F, Merchán M, Robb MA, Olivucci M (2000) Computational evidence in favor of a two-state, two-mode model of the retinal chromophore photoisomerization. Proc Natl Acad Sci USA 97:9379–9384
Govorunova EG, Cunha SR, Sineshchekov OA, Spudich JL (2016) Anion channelrhodopsins for inhibitory cardiac optogenetics. Sci Rep 6:33530
Govorunova EG, Sineshchekov OA, Li H, Spudich JL (2017) Microbial rhodopsins: diversity, mechanisms, and optogenetic applications. Annu Rev Biochem 86:845–872
Gozem S, Luk HL, Schapiro I, Olivucci M (2017) Theory and simulation of the ultrafast double-bond isomerization of biological chromophores. Chem Rev 117:13502–13565
Grossfield A (2008) Implicit modeling of membranes. Curr Top Membr 60:131–157
Grossfield A (2011) Recent progress in the study of G protein-coupled receptors with molecular dynamics computer simulations. Biochim Biophys Acta 1808:1868–1878
Grossfield A, Feller SE, Pitman MC (2006a) Contribution of omega-3 fatty acids to the thermodynamics of membrane protein solvation. J Phys Chem B 110:8907–8909
Grossfield A, Feller SE, Pitman MC (2006b) A role for direct interactions in the modulation of rhodopsin by $\omega$-3 polyunsaturated lipids. Proc Natl Acad Sci USA 103:4888–4893
Guo Y, Beyle FE, Bold BM, Watanabe HC, Koslowski A, Thiel W, Hegemann P, Marazzi M, Elstner M (2016) Active site structure and absorption spectrum of channelrhodopsin-2 wild-type and C128T mutant. Chem Sci 7:3879–3891
Gushchin I, Gordeliy V, Grudinin S (2013) Two distinct states of the HAMP domain from sensory rhodopsin transducer observed in unbiased molecular dynamics simulations. PLoS ONE 8:e66917
Gushchin I, Shevchenko V, Polovinkin V, Kovalev K, Alekseev A, Round E, Borshchevskiy V, Balandin T, Popov A, Gensch T, Fahlke C, Baumann C, Willbold D, Büldt G, Bamberg E, Gordelly V (2015) Crystal structure of a light-driven sodium pump. Nat Struct Mol Biol 22:390–395
Gutiérrez-de-Terán H, Massink A, Rodríguez D, Liu W, Han GW, Joseph JS, Katritch I, Heitman LH, Xia L, IJzerman AP, Cherezov V, Katritch V, Stevens RC (2013) The role of a sodium ion binding site in the allosteric modulation of the $A_{2A}$ adenosine G protein-coupled receptor. Structure 21:2175–2185
Hall KF, Vreven T, Frisch MJ, Bearpark MJ (2008) Three-layer ONIOM studies of the dark state of rhodopsin: the protonation state of Glu181. J Mol Biol 383:106–121
Hamanaka T, Mitsui T, Ashida T, Kakudo M (1972) The crystal structure of all-*trans* retinal$_1$. Acta Crystallogr B 28:214–222
Hansen N, Van Gunsteren WF (2014) Practical aspects of free-energy calculations: a review. J Chem Theory Comput 10:2632–2647

Harbison GS, Roberts JE, Herzfeld J, Griffin RG (1988) Solid-state NMR detection of proton exchange between the bacteriorhodopsin Schiff base and bulk water. J Am Chem Soc 110:7221–7223

Hayashi S, Tajkhorshid E, Schulten K (2002) Structural changes during the formation of early intermediates in the bacteriorhodopsin photocycle. Biophys J 83:1281–1297

Hein M, Wegener AA, Engelhard M, Siebert F (2003) Time-resolved FTIR studies of sensory rhodopsin II (NpSRII) from *Natronobacterium pharaonis*: implications for proton transport and receptor activation. Biophys J 84:1208–1217

Hénin J, Maigret B, Tarek M, Escrieut C, Fourmy D, Chipot C (2006) Probing a model of a GPCR/ligand complex in an explicit membrane environment: the human cholecystokinin-1 receptor. Biophys J 90:1232–1240

Hill JR, Deane CM (2012) MP-T: improving membrane protein alignment for structure prediction. Bioinformatics 29:54–61

Hillebrecht JR, Galan J, Rangarajan R, Ramos L, McCleary K, Ward DE, Stuart JA, Birge RR (2006) Structure, function, and wavelength selection in blue-absorbing proteorhodopsin. Biochemistry 45:1579–1590

Hochbaum DR, Zhao Y, Farhi SL, Klapoetke N, Werley CA, Kapoor V, Zou P, Kralj JM, Maclaurin D, Smedemark-Margulies N (2014) All-optical electrophysiology in mammalian neurons using engineered microbial rhodopsins. Nat Methods 11:825–833

Hoffmann M, Wanko M, Strodel P, König PH, Frauenheim T, Schulten K, Thiel W, Tajkhorshid E, Elstner M (2006) Color tuning in rhodopsins: the mechanism for the spectral shift between bacteriorhodopsin and sensory rhodopsin II. J Am Chem Soc 128:10808–10818

Horn JN, Kao T-C, Grossfield A (2014) Coarse-grained molecular dynamics provides insight into the interactions of lipids and cholesterol with rhodopsin. Adv Exp Med Biol 796:75–94

Hornak V, Ahuja S, Eilers M, Goncalves JA, Sheves M, Reeves PJ, Smith SO (2010) Light activation of rhodopsin: insights from molecular dynamics simulations guided by solid-state NMR distance restraints. J Mol Biol 396:510–527

Huang W, Manglik A, Venkatakrishnan AJ, Laeremans T, Feinberg EN, Sanborn AL, Kato HE, Livingston KE, Thorsen TS, Kling RC, Granier S, Gmeiner P, Husbands SM, Traynor JR, Weiss WI, Steyaert J, Dror RO, Kobilka BK (2015) Structural insights into $\mu$-opioid receptor activation. Nature 524:315–321

Huber T, Sakmar TP (2008) Rhodopsin's active state is frozen like a DEER in the headlights. Proc Natl Acad Sci USA 105:7343–7344

Huber T, Botelho AV, Beyer K, Brown MF (2004) Membrane model for the G-protein-coupled receptor rhodopsin: hydrophobic interface and dynamical structure. Biophys J 86:2078–2100

Im W, Feig M, Brooks CL III (2003) An implicit membrane generalized Born theory for the study of structure, stability, and interactions of membrane proteins. Biophys J 85:2900–2918

Isralewitz B, Izrailev S, Schulten K (1997) Binding pathway of retinal to bacterio-opsin: a prediction by molecular dynamics simulations. Biophys J 73:2972–2979

Izvekov S, Voth GA (2005) A multiscale coarse-graining method for biomolecular systems. J Phys Chem B 109:2469–2473

Jämbeck JP, Lyubartsev AP (2012) An extension and further validation of an all-atomistic force field for biological membranes. J Chem Theory Comput 8:2938–2948

Jardón-Valadez E, Bondar A-N, Tobias DJ (2010) Coupling of retinal, protein, and water dynamics in squid rhodopsin. Biophys J 99:2200–2207

Jarzynski C (1997) Equilibrium free-energy differences from nonequilibrium measurements: a master-equation approach. Phys Rev E 56:5018

Jensen MR, Zweckstetter M, Huang J-r, Blackledge M (2014) Exploring free-energy landscapes of intrinsically disordered proteins at atomic resolution using NMR spectroscopy. Chem Rev 114:6632–6660

Johnston JM, Wang H, Provasi D, Filizola M (2012) Assessing the relative stability of dimer interfaces in G protein-coupled receptors. PLoS Comput Biol 8:e1002649

Kaminski GA, Friesner RA, Tirado-Rives J, Jorgensen WL (2001) Evaluation and reparametrization of the OPLS-AA force field for proteins via comparison with accurate quantum chemical calculations on peptides. J Phys Chem B 105:6474–6487

Kästner J (2011) Umbrella sampling. Wiley Interdiscip Rev 1:932–942

Kaszuba K, Róg T, Bryl K, Vattulainen I, Karttunen M (2010) Molecular dynamics simulations reveal fundamental role of water as factor determining affinity of binding of $\beta$-blocker nebivolol to $\beta_2$-adrenergic receptor. J Phys Chem B 114:8374–8386

Kaufmann KW, Lemmon GH, DeLuca SL, Sheehan JH, Meiler J (2010) Practically useful: what the Rosetta protein modeling suite can do for you. Biochemistry 49:2987–2998

Kazmin R, Rose A, Szczepek M, Elgeti M, Ritter E, Piechnick R, Hofmann KP, Scheerer P, Hildebrand PW, Bartl FJ (2015) The activation pathway of human rhodopsin in comparison to bovine rhodopsin. J Biol Chem 290:20117–201127

Kelm S, Shi J, Deane CM (2010) MEDELLER: homology-based coordinate generation for membrane proteins. Bioinformatics 26:2833–2840

Khan FI, Wei D-Q, Gu K-R, Hassan MI, Tabrez S (2016) Current updates on computer aided protein modeling and designing. Int J Biol Macromol 85:48–62

Khandogin J, Brooks CL (2005) Constant pH molecular dynamics with proton tautomerism. Biophys J 89:141–157

Khelashvili G, Albornoz PBC, Johner N, Mondal S, Caffrey M, Weinstein H (2012) Why GPCRs behave differently in cubic and lamellar lipidic mesophases. J Am Chem Soc 134:15858–15868

Kholmurodov KT, Fel'dman T, Ostrovskii M (2007) Molecular dynamics of rhodopsin and free opsin: computer simulation. Neurosci Behav Physiol 37:161–174

Khrenova MG, Bochenkova AV, Nemukhin AV (2010) Modeling reaction routes from rhodopsin to bathorhodopsin. Proteins 78:614–622

Kilambi KP, Gray JJ (2012) Rapid calculation of protein p$K_a$ values using Rosetta. Biophys J 103:587–595

Klauda JB, Venable RM, Freites JA, O'Connor JW, Tobias DJ, Mondragon-Ramirez C, Vorobyov I, MacKerell AD Jr, Pastor RW (2010) Update of the CHARMM all-atom additive force field for lipids: validation on six lipid types. J Phys Chem B 114:7830–7843

Krebs A, Edwards PC, Villa C, Li J, Schertler GFX (2003) The three-dimensional structure of bovine rhodopsin determined by electron cryomicroscopy. J Biol Chem 278:50217–50225

Kukura P, McCamant DW, Yoon S, Wandschneider DB, Mathies RA (2005) Structural observation of the primary isomerization in vision with femtosecond-stimulated Raman. Science 310:1006–1009

Kumar S, Rosenberg JM, Bouzida D, Swendsen RH, Kollman PA (1992) The weighted histogram analysis method for free-energy calculations on biomolecules. I. The method. J Comput Chem 13:1011–1021

Laio A, Gervasio FL (2008) Metadynamics: a method to simulate rare events and reconstruct the free energy in biophysics, chemistry and material science. Rep Prog Phys 71:126601

Laio A, Parrinello M (2002) Escaping free-energy minima. Proc Natl Acad Sci USA 99:12562–12566

Latorraca NR, Venkatakrishnan A, Dror RO (2017) GPCR dynamics: structures in motion. Chem Rev 117:139–155

Latorraca NR, Wang JK, Bauer B, Townshend RJ, Hollingsworth SA, Olivieri JE, Xu HE, Sommer ME, Dror RO (2018) Molecular mechanism of GPCR-mediated arrestin activation. Nature 557:452–456

Lau P-W, Grossfield A, Feller SE, Pitman MC, Brown MF (2007) Dynamic structure of retinylidene ligand of rhodopsin probed by molecular simulations. J Mol Biol 372:906–917

Lee J, Freddolino PL, Zhang Y (2017) Ab initio protein structure prediction. In: Daniel JR (ed) From Protein Structure to Function with Bioinformatics. Springer, Berlin, pp 3–35

Leguèbe M, Nguyen C, Capece L, Hoang Z, Giorgetti A, Carloni P (2012) Hybrid molecular mechanics/coarse-grained simulations for structural prediction of G-protein coupled receptor/ligand complexes. PLoS ONE 7:e47332

Leioatts N, Mertz B, Martínez-Mayorga K, Romo TD, Pitman MC, Feller SE, Grossfield A, Brown MF (2014) Retinal ligand mobility explains internal hydration and reconciles active rhodopsin structures. Biochemistry 53:376–385

Lemaître V, Yeagle P, Watts A (2005) Molecular dynamics simulations of retinal in rhodopsin: from the dark-adapted state towards lumirhodopsin. Biochemistry 44:12667–12680

Lenselink EB, Louvel J, Forti AF, van Veldhoven JPD, de Vries H, Mulder-Krieger T, McRobb FM, Negri A, Goose J, Abel R, van Vlijmen HWT, Wang L, Harder E, Sherman W, IJzerman AP, Beuming T (2016) Predicting binding affinities for GPCR ligands using free-energy perturbation. ACS Omega 1:293–304

Leonard AN, Pastor RW, Klauda JB (2018) Parameterization of the CHARMM all-atom force field for ether lipids and model linear ethers. J Phys Chem B 122:6744–6754

Li X, Chung LW, Morokuma K (2011) Photodynamics of all-*trans* retinal protonated Schiff base in bacteriorhodopsin and methanol solution. J Chem Theory Comput 7:2694–2698

Lin H, Truhlar DG (2007) QM/MM: what have we learned, where are we, and where do we go from here? Theoret Chem Acc 117:185–199

Lindorff-Larsen K, Piana S, Palmo K, Maragakis P, Klepeis JL, Dror RO, Shaw DE (2010) Improved side-chain torsion potentials for the Amber ff99SB protein force field. Proteins 78:1950–1958

Lischka H, Dallos M, Shepard R (2002) Analytic MRCI gradient for excited states: formalism and application to the n-$\pi^*$ valence- and n-(3s, 3p) Rydberg states of formaldehyde. Mol Phys 100:1647–1658

Mackerell AD Jr, Feig M, Brooks CL III (2004) Extending the treatment of backbone energetics in protein force fields: limitations of gas-phase quantum mechanics in reproducing protein conformational distributions in molecular dynamics simulations. J Comput Chem 25:1400–1415

Maclaurin D, Venkatachalam V, Lee H, Cohen AE (2013) Mechanism of voltage-sensitive fluorescence in a microbial rhodopsin. Proc Natl Acad Sci USA 110:5939–5944

Marchiori A, Capece L, Giorgetti A, Gasparini P, Behrens M, Carloni P, Meyerhof W (2013) Coarse-grained/molecular mechanics of the TAS2R38 bitter taste receptor: experimentally-validated detailed structural prediction of agonist binding. PLoS ONE 8:e64675

Marrink SJ, De Vries AH, Mark AE (2004) Coarse grained model for semiquantitative lipid simulations. J Phys Chem B 108:750–760

Marrink SJ, Risselada HJ, Yefimov S, Tieleman DP, De Vries AH (2007) The MARTINI force field: coarse grained model for biomolecular simulations. J Phys Chem B 111:7812–7824

Martínez-Mayorga K, Pitman MC, Grossfield A, Feller SE, Brown MF (2006) Retinal counterion switch mechanism in vision evaluated by molecular simulations. J Am Chem Soc 128:16502–16503

Melaccio F, Ferré N, Olivucci M (2012) Quantum chemical modeling of rhodopsin mutants displaying switchable colors. Phys Chem Chem Phys 14:12485–12495

Meral D, Provasi D, Filizola M (2018) An efficient strategy to estimate thermodynamics and kinetics of G protein-coupled receptor activation using metadynamics and maximum caliber. J Chem Phys 149:224101

Mertz B, Lu M, Brown MF, Feller SE (2011) Steric and electronic influences on the torsional energy landscape of retinal. Biophys J 101:L17–L19

Mertz B, Struts AV, Feller SE, Brown MF (2012) Molecular simulations and solid-state NMR investigate dynamical structure in rhodopsin activation. Biochem Biophys Acta 1818:241–251

Metropolis N, Ulam S (1949) The Monte Carlo method. J Am Stat Assoc 44:335–341

Miao Y, Caliman AD, McCammon JA (2015) Allosteric effects of sodium ion binding on activation of the M3 muscarinic G-protein-coupled receptor. Biophys J 108:1796–1806

Monticelli L, Kandasamy SK, Periole X, Larson RG, Tieleman DP, Marrink S-J (2008) The MARTINI coarse-grained force field: extension to proteins. J Chem Theory Comput 4:819–834

Moradi M, Babin V, Sagui C, Roland C (2013) Recipes for free energy calculations in biomolecular systems. Methods Mol Biol 924:313–337

Mori T, Miyashita N, Im W, Feig M, Sugita Y (2016) Molecular dynamics simulations of biological membranes and membrane proteins using enhanced conformational sampling algorithms. Biochim Biophys Acta 1858:1635–1651

Morozenko A, Stuchebrukhov A (2016) Dowser++, a new method of hydrating protein structures. Proteins 84:1347–1357

Morozenko A, Leontyev I, Stuchebrukhov A (2014) Dipole moment and binding energy of water in proteins from crystallographic analysis. J Chem Theory Comput 10:4618–4623

Nielsen IB, Lammich L, Andersen LH (2006) $S_1$ and $S_2$ excited states of gas-phase Schiff-base retinal chromophores. Phys Rev Lett 96:018304

Nikolaev DM, Emelyanov A, Boitsov VM, Panov MS, Ryazantsev MN (2017) A voltage-dependent fluorescent indicator for optogenetic applications, archaerhodopsin-3: structure and optical properties from in silico modeling. F1000Research 6:33

Nikolaev DM, Shtyrov AA, Panov MS, Jamal A, Chakchir OB, Kochemirovsky VA, Olivucci M, Ryazantsev MN (2018) A comparative study of modern homology modeling algorithms for rhodopsin structure prediction. ACS Omega 3:7555–7566

Nikolaev DM, Osipov DE, Strashkov DM, Vyazmin SY, Akulov VE, Kravtcov DV, Chakchir OB, Panov MS, Ryazantsev MN (2019a) Molecular mechanisms of adaptation to the habitat depth in visual pigments of *A. subulata* and *L. forbesi* squids: on the role of the S270F substitution. J Integr OMICS 9:44–50

Nikolaev DM, Panov MS, Shtyrov AA, Boitsov VM, Vyazmin SY, Chakchir OB, Yakovlev IP, Ryazantsev MN (2019b) Perspective tools for optogenetics and photopharmacology: from design to implementation. In: Yamanouchi K, Tunik S, Makarov V (eds) Progress in Photon Science. Springer, Berlin, pp 139–172

Nina M, Roux B, Smith JC (1995) Functional interactions in bacteriorhodopsin: a theoretical analysis of retinal hydrogen bonding with water. Biophys J 68:25–39

Noid W (2013) Systematic methods for structurally consistent coarse-grained models. Methods Mol Biol 924:487–531

Nygaard R, Zou Y, Dror RO, Mildorf TJ, Arlow DH, Manglik A, Pan AC, Liu CW, Fung JJ, Bokoch MP, Thian FS, Kobilka TS, Shaw DE, Mueller L, Prosser RS, Kobilka BK (2013) The dynamic process of $\beta_2$-adrenergic receptor activation. Cell 152:532–542

Okuyama-Yoshida N, Kataoka K, Nagaoka M, Yamabe T (2000) Structure optimization via free energy gradient method: application to glycine zwitterion in aqueous solution. J Chem Phys 113:3519–3524

Olausson BE, Grossfield A, Pitman MC, Brown MF, Feller SE, Vogel A (2012) Molecular dynamics simulations reveal specific interactions of post-translational palmitoyl modifications with rhodopsin in membranes. J Am Chem Soc 134:4324–4331

Olsson MHM, Søndergaard CR, Rostkowski M, Jensen JH (2011) PROPKA3: consistent treatment of internal and surface residues in empirical p$K_a$ predictions. J Chem Theory Comput 7:525–537

Oostenbrink C, Villa A, Mark AE, Van Gunsteren WF (2004) A biomolecular force field based on the free enthalpy of hydration and solvation: the GROMOS force-field parameter sets 53A5 and 53A6. J Comput Chem 25:1656–1676

Orozco-Gonzalez Y, Manathunga M, Marin MdC, Agathangelou D, Jung KH, Melaccio F, Ferré N, Haacke S, Coutinho K, Canuto S, Olivucci M (2017) An average solvent electrostatic configuration protocol for QM/MM free energy optimization: implementation and application to rhodopsin systems. J Chem Theory Comput 13:6391–6404

Pastor R, MacKerell AD Jr (2011) Development of the CHARMM force field for lipids. J Phys Chem Lett 2:1526–1532

Patel AB, Crocker E, Eilers M, Hirshfeld A, Sheves M, Smith SO (2004) Coupling of retinal isomerization to the activation of rhodopsin. Proc Natl Acad Sci USA 101:10048–10053

Perera SM, Chawla U, Shrestha UR, Bhowmik D, Struts AV, Qian S, Chu X-Q, Brown MF (2018) Small-angle neutron scattering reveals energy landscape for rhodopsin photoactivation. J Phys Chem Lett 9:7064–7071

Periole X (2016) Interplay of G protein-coupled receptors with the membrane: insights from supra-atomic coarse grain molecular dynamics simulations. Chem Rev 117:156–185

Periole X, Huber T, Marrink S-J, Sakmar TP (2007) G protein-coupled receptors self-assemble in dynamics simulations of model bilayers. J Am Chem Soc 129:10126–10132

Periole X, Knepp AM, Sakmar TP, Marrink SJ, Huber T (2012) Structural determinants of the supramolecular organization of G protein-coupled receptors in bilayers. J Am Chem Soc 134:10959–10965

Provasi D, Filizola M (2010) Putative active states of a prototypic G-protein-coupled receptor from biased molecular dynamics. Biophys J 98:2347–2355

Provasi D, Palczewski K, Filizola M (2009) Exploring the thermodynamics of activation pathways of bovine rhodopsin with fast molecular dynamics simulations. Biophys J 96:679a

Raiteri P, Laio A, Gervasio FL, Micheletti C, Parrinello M (2006) Efficient reconstruction of complex free energy landscapes by multiple walkers metadynamics. J Phys Chem B 110:3533–3539

Rajamani R, Gao J (2002) Combined QM/MM study of the opsin shift in bacteriorhodopsin. J Comput Chem 23:96–105

Richards R, Dempski RE (2017) Adjacent channelrhodopsin-2 residues within transmembranes 2 and 7 regulate cation selectivity and distribution of the two open states. J Biol Chem 292:7314–7326

Rinaldi S, Melaccio F, Gozem S, Fanelli F, Olivucci M (2014) Comparison of the isomerization mechanisms of human melanopsin and invertebrate and vertebrate rhodopsins. Proc Natl Acad Sci USA 111:1714–1719

Romo TD, Grossfield A, Pitman MC (2010) Concerted interconversion between ionic lock substates of the $\beta_2$ adrenergic receptor revealed by microsecond timescale molecular dynamics. Biophys J 98:76–84

Ross GA, Morris GM, Biggin PC (2012) Rapid and accurate prediction and scoring of water molecules in protein binding sites. PLoS ONE 7:e32036

Rostkowski M, Olsson MHM, Søndergaard CR, Jensen JH (2011) Graphical analysis of pH-dependent properties of proteins predicted using PROPKA. BMC Struct Biol 11:6

Rotov AY, Astakhova L, Sitnikova V, Evdokimov A, Boitsov V, Dubina M, Ryazantsev M, Firsov M (2018) New experimental models of retinal degeneration for screening molecular photochromic ion channel blockers. Acta Nat 10:75–84

Roux B, Nina M, Pomès R, Smith JC (1996) Thermodynamic stability of water molecules in the bacteriorhodopsin proton channel: a molecular dynamics free energy perturbation study. Biophys J 71:670–681

Roy A, Kucukural A, Zhang Y (2010) I-TASSER: a unified platform for automated protein structure and function prediction. Nat Protoc 5:725–738

Ryazantsev MN, Altun A, Morokuma K (2012) Color tuning in rhodopsins: the origin of the spectral shift between the chloride-bound and anion-free forms of halorhodopsin. J Am Chem Soc 134:5520–5523

Saam J, Tajkhorshid E, Hayashi S, Schulten K (2002) Molecular dynamics investigation of primary photoinduced events in the activation of rhodopsin. Biophys J 83:3097–3112

Sahoo BR, Genjo T, Maharana KC, Ramamoorthy A (2019) Self-assembly of polymer-encased lipid nanodiscs and membrane protein reconstitution. J Phys Chem B 123:4562–4570

Saint Clair EC, Ogren JI, Mamaev S, Kralj JM, Rothschild KJ (2012a) Conformational changes in the archaerhodopsin-3 proton pump: detection of conserved strongly hydrogen bonded water networks. J Biol Phys 38:153–168

Saint Clair EC, Ogren JI, Mamaev S, Russano D, Kralj JM, Rothschild KJ (2012b) Near-IR resonance Raman spectroscopy of archaerhodopsin 3: effects of transmembrane potential. J Phys Chem B 116:14592–14601

Sakmar TP, Periole X, Huber T (2017) Probing self-assembly of G protein-coupled receptor oligomers in membranes using molecular dynamics modeling and experimental approaches. In: Herrick-Davis K, Milligan G, Di Giovanni G (eds) G-Protein-Coupled Receptor Dimers. Humana Press, Cham, pp 385–414

Salamon Z, Brown MF, Tollin G (1999) Plasmon resonance spectroscopy: probing molecular interactions within membranes. Trends Biochem Sci 24:213–219

Salas-Estrada LA, Leioatts N, Romo TD, Grossfield A (2018) Lipids alter rhodopsin function via ligand-like and solvent-like interactions. Biophys J 114:355–367

Saleh N, Ibrahim P, Saladino G, Gervasio FL, Clark T (2017) An efficient metadynamics-based protocol to model the binding affinity and the transition state ensemble of G-protein-coupled receptor ligands. J Chem Inf Model 57:1210–1217

Saunders MG, Voth GA (2013) Coarse-graining methods for computational biology. Ann Rev Biophys 42:73–93

Schaefer P, Riccardi D, Cui Q (2005) Reliable treatment of electrostatics in combined QM/MM simulation of macromolecules. J Chem Phys 123:014905

Schapiro I, Weingart O, Buss V (2008) Bicycle-pedal isomerization in a rhodopsin chromophore model. J Am Chem Soc 131:16–17

Schapiro I, Ryazantsev MN, Frutos LM, Ferré N, Lindh R, Olivucci M (2011) The ultrafast photoisomerizations of rhodopsin and bathorhodopsin are modulated by bond length alternation and HOOP driven electronic effects. J Am Chem Soc 133:3354–3364

Schmidt TH, Kandt C (2012) LAMBADA and InflateGRO2: efficient membrane alignment and insertion of membrane proteins for molecular dynamics simulations. J Chem Inf Model 52:2657–2669

Schnedermann C, Yang X, Liebel M, Spillane K, Lugtenburg J, Fernández I, Valentini A, Schapiro I, Olivucci M, Kukura P, Mathies RA (2018) Evidence for a vibrational phase-dependent isotope effect on the photochemistry of vision. Nat Chem 10:449–455

Schoenlein RW, Peteanu LA, Mathies RA, Shank CV (1991) The first step in vision: femtosecond isomerization of rhodopsin. Science 254:412–415

Scott KA, Bond PJ, Ivetac A, Chetwynd AP, Khalid S, Sansom MS (2008) Coarse-grained MD simulations of membrane protein-bilayer self-assembly. Structure 16:621–630

Senn HM, Thiel W (2009) QM/MM methods for biomolecular systems. Angew Chem Int Ed 48:1198–1229

Shirts MR, Mobley DL (2013) An introduction to best practices in free energy calculations. Methods Mol Biol 924:271–311

Shrestha UR, Perera SM, Bhowmik D, Chawla U, Mamontov E, Brown MF, Chu X-Q (2016) Quasi-elastic neutron scattering reveals ligand-induced protein dynamics of a G-protein-coupled receptor. J Phys Chem Lett 7:4130–4136

Simonson T, Carlsson J, Case DA (2004) Proton binding to proteins: p$K_a$ calculations with explicit and implicit solvent models. J Am Chem Soc 126:4167–4180

Smith SO (2010) Structure and activation of the visual pigment rhodopsin. Ann Rev Biophys 39:309–328

Söderhjelm P, Husberg C, Strambi A, Olivucci M, Ryde U (2009) Protein influence on electronic spectra modeled by multipoles and polarizabilities. J Chem Theory Comput 5:649–658

Söding J (2004) Protein homology detection by HMM–HMM comparison. Bioinformatics 21:951–960

Song Y, DiMaio F, Wang RY-R, Kim D, Miles C, Brunette TJ, Thompson J, Baker D (2013) High-resolution comparative modeling with RosettaCM. Structure 21:1735–1742

Sridhar A, Ross GA, Biggin PC (2017) Waterdock 2.0: water placement prediction for holo-structures with a PYMOL plugin. PLoS ONE 12:e0172743

Standfuss J, Edwards PC, D'Antona A, Fransen M, Xie G, Oprian DD, Schertler GFX (2011) The structural basis of agonist-induced activation in constitutively active rhodopsin. Nature 471:656–660

Strambi A, Coto PB, Frutos LM, Ferré N, Olivucci M (2008) Relationship between the excited state relaxation paths of rhodopsin and isorhodopsin. J Am Chem Soc 130:3382–3388

Struts AV, Salgado GF, Brown MF (2011) Solid-state $^2$H NMR relaxation illuminates functional dynamics of retinal cofactor in membrane activation of rhodopsin. Proc Natl Acad Sci USA 108:8263–8268

Sumita M, Ryazantsev MN, Saito K (2009) Acceleration of the Z to E photoisomerization of penta-2,4-dieniminium by hydrogen out-of-plane motion: theoretical study on a model system of retinal protonated Schiff base. Phys Chem Chem Phys 11:6406–6414

Suomivuori C-M, Gamiz-Hernandez AP, Sundholm D, Kaila VR (2017) Energetics and dynamics of a light-driven sodium-pumping rhodopsin. Proc Natl Acad Sci USA 114:7043–7048

Svensson M, Humbel S, Froese RDJ, Matsubara T, Sieber S, Morokuma K (1996) ONIOM: a multilayered integrated MO + MM method for geometry optimizations and single point energy predictions. A test for Diels–Alder reactions and Pt(P($t$-Bu)$_3$)$_2$ + H$_2$ oxidative addition. J Phys Chem 100:19357–19363

Tajkhorshid E, Suhai S (2000) The dielectric effect of the environment on the p$K_a$ of the retinal Schiff base and on the stabilization of the ion pair in bacteriorhodopsin. J Mol Struct: THEOCHEM 501:297–313

Tajkhorshid E, Paizs B, Suhai S (1997) Conformational effects on the proton affinity of the Schiff base in bacteriorhodopsin: a density functional study. J Phys Chem B 101:8021–8028

Tajkhorshid E, Baudry J, Schulten K, Suhai S (2000) Molecular dynamics study of the nature and origin of retinal's twisted structure in bacteriorhodopsin. Biophys J 78:683–693

Takemoto M, Kato HE, Koyama M, Ito J, Kamiya M, Hayashi S, Maturana AD, Deisseroth K, Ishitani R, Nureki O (2015) Molecular dynamics of channelrhodopsin at the early stages of channel opening. PLoS ONE 10:e0131094

Tavanti F, Tozzini V (2014) A multi-scale–multi-stable model for the rhodopsin photocycle. Molecules 19:14961–14978

Thomas YG, Szundi I, Lewis JW, Kliger DS (2009) Microsecond time-resolved circular dichroism of rhodopsin photointermediates. Biochemistry 48:12283–12289

Tikhonova IG, Selvam B, Ivetac A, Wereszczynski J, McCammon JA (2013) Simulations of biased agonists in the $\beta_2$ adrenergic receptor with accelerated molecular dynamics. Biochemistry 52:5593–5603

Tomasello G, Olaso-González G, Altoè P, Stenta M, Serrano-Andrés L, Merchán M, Orlandi G, Bottoni A, Garavelli M (2009) Electrostatic control of the photoisomerization efficiency and optical properties in visual pigments: on the role of counterion quenching. J Am Chem Soc 131:5172–5186

Trott O, Olson AJ (2010) AutoDock Vina: improving the speed and accuracy of docking with a new scoring function, efficient optimization, and multithreading. J Comput Chem 31:455–461

Ulmschneider JP, Ulmschneider MB (2009) Sampling efficiency in explicit and implicit membrane environments studied by peptide folding simulations. Proteins 75:586–597

Van Keulen SC, Solano A, Rothlisberger U (2017) How rhodopsin tunes the equilibrium between protonated and deprotonated forms of the retinal chromophore. J Chem Theory Comput 13:4524–4534

Vanni S, Neri M, Tavernelli I, Rothlisberger U (2010) A conserved protonation-induced switch can trigger "ionic-lock" formation in adrenergic receptors. J Mol Biol 397:1339–1349

Vanommeslaeghe K, Hatcher E, Acharya C, Kundu S, Zhong S, Shim J, Darian E, Guvench O, Lopes P, Vorobyov I, Mackerell AD Jr (2010) CHARMM general force field: a force field for drug-like molecules compatible with the CHARMM all-atom additive biological force fields. J Comput Chem 31:671–690

Vickery ON, Carvalheda CA, Zaidi SA, Pisliakov AV, Katritch V, Zachariae U (2018) Intracellular transfer of $Na^+$ in an active-state G-protein-coupled receptor. Structure 26:171–180

Volkov O, Kovalev K, Polovinkin V, Borshchevskiy V, Bamann C, Astashkin R, Marin E, Popov A, Balandin T, Willbold D, Büldt G, Bamberg E, Gordelly V (2017) Structural insights into ion conduction by channelrhodopsin 2. Science 358:eaan8862

Vreven T, Morokuma K (2006) Hybrid methods: ONIOM (QM:MM) and QM/MM. Ann Rep Comput Chem 2:35–51

Vyěmtal J, Vondrášek J (2010) Metadynamics as a tool for mapping the conformational and free-energy space of peptides—the alanine dipeptide case study. J Phys Chem B 114:5632–5642

Wacker D, Wang S, McCorvy JD, Betz RM, Venkatakrishnan A, Levit A, Lansu K, Schools ZL, Che T, Nichols DE, Shoiket BK, Dror RO, Roth BL (2017) Crystal structure of an LSD-bound human serotonin receptor. Cell 168:379–389

Wang Q, Schoenlein RW, Peteanu LA, Mathies RA, Shank CV (1994) Vibrationally coherent photochemistry in the femtosecond primary event of vision. Science 266:422–424

Wang J, Wolf RM, Caldwell JW, Kollman PA, Case DA (2004) Development and testing of a general Amber force field. J Comput Chem 25:1157–1174

Wang L-P, Chen J, Van Voorhis T (2012) Systematic parametrization of polarizable force fields from quantum chemistry data. J Chem Theory Comput 9:452–460

Wanko M, Hoffmann M, Frähmcke J, Frauenheim T, Elstner M (2008a) Effect of polarization on the opsin shift in rhodopsins. 2. Empirical polarization models for proteins. J Phys Chem B 112:11468–11478

Wanko M, Hoffmann M, Frauenheim T, Elstner M (2008b) Effect of polarization on the opsin shift in rhodopsins. 1. A combined QM/QM/MM model for bacteriorhodopsin and *pharaonis* sensory rhodopsin II. J Phys Chem B 112:11462–11467

Warshel A, Chu Z (2001) Nature of the surface crossing process in bacteriorhodopsin: computer simulations of the quantum dynamics of the primary photochemical event. J Phys Chem B 105:9857–9871

Weis WI, Kobilka BK (2018) The molecular basis of G protein–coupled receptor activation. Annu Rev Biochem 87:897–919

Wu S, Zhang Y (2008) MUSTER: improving protein sequence profile–profile alignments by using multiple sources of structure information. Proteins 72:547–556

Wu S, Skolnick J, Zhang Y (2007) Ab initio modeling of small proteins by iterative TASSER simulations. BMC Biol 5:17

Xu D, Zhang Y (2011) Improving the physical realism and structural accuracy of protein models by a two-step atomic-level energy minimization. Biophys J 101:2525–2534

Yamada T, Yamato T, Mitaku S (2016) Forced unfolding mechanism of bacteriorhodopsin as revealed by coarse-grained molecular dynamics. Biophys J 111:2086–2098

Yang J, Zhang Y (2015) I-TASSER server: new development for protein structure and function predictions. Nucl Acids Res 43:W174–W181

Yang J, Yan R, Roy A, Xu D, Poisson J, Zhang Y (2015) The I-TASSER suite: protein structure and function prediction. Nat Methods 12:7–8

Ye L, Neale C, Sljoka A, Lyda B, Pichugin D, Tsuchimura N, Larda ST, Pomès R, García AE, Ernst OP, Sunahara RK, Prosser RS (2018) Mechanistic insights into allosteric regulation of the $A_{2A}$ adenosine G protein-coupled receptor by physiological cations. Nat Commun 9:1372

Yuan S, Filipek S, Palczewski K, Vogel H (2014) Activation of G-protein-coupled receptors correlates with the formation of a continuous internal water pathway. Nat Commun 5:4733

Zhang L, Hermans J (1996) Hydrophilicity of cavities in proteins. Proteins 24:433–438

Zhang Y, Skolnick J (2004) SPICKER: a clustering approach to identify near-native protein folds. J Comput Chem 25:865–871

Zhou F, Windemuth A, Schulten K (1993) Molecular dynamics study of the proton pump cycle of bacteriorhodopsin. Biochemistry 32:2291–2306

Zhou X, Sundholm D, Wesołowski TA, Kaila VR (2014) Spectral tuning of rhodopsin and visual cone pigments. J Am Chem Soc 136:2723–2726

Zhu S, Brown MF, Feller SE (2013) Retinal conformation governs p$K_a$ of protonated Schiff base in rhodopsin activation. J Am Chem Soc 135:9391–9398

Zwanzig RW (1954) High-temperature equation of state by a perturbation method. I. Nonpolar gases. J Chem Phys 22:1420–1426